



School of Chemistry

**Optimizing the Secondary Electron Emission
Yield (SEELY) of Diamond Self-Assemblies**

Stella Papadopoulos

Dr. Neil Fox

Professor David Fermin

Physical and Theoretical Chemistry

Acknowledgement

First and foremost, I would like to express my deepest gratitude to my supervisor, Dr. Neil Fox. His enthusiasm and patience made my research experience highly enjoyable and his depth of knowledge inspired me to widen my understanding of the area and work as hard as I could.

I would like to thank everyone in the Diamond Group for their help around the lab and their willingness to answer any questions I had.

I extend my thanks to Dr. Sean Davis, who helped me with the SEM images, and Dr. Richard Schubert-Rowles for his help in the Krüss lab.

Finally, I could not have completed this project to the best of my ability without the love and support of my family, friends and partner.

Thank you all!

Stella

Abstract

An investigation into the optimum layers for diamond self-assemblies was undertaken with the aim to maximise the secondary electron emission yield (SEY). Three metal substrates: BeCu, Ag and Ni, formed the base, for which the oxidation times were varied. Analysis of two polymers: carboxylethyl silanetriol sodium salt and poly(ethyleneimine), and modification of the concentration of the latter polymer was performed. All the samples were OLi-terminated, establishing a negative electron affinity surface. Research has demonstrated that this type of surface yields a high secondary electron emission. A conclusion was drawn following an examination of the contact angle measurements, the morphology and fractional coverage of the surface and the SEY. The BeCu oxidised for 30 minutes was the optimal metal substrate. Due to equipment error, a quantitative conclusion was unable to be made with respect to the favourable polymer and its concentration. A prediction, however, was deduced that the self-assembled sample using the poly(ethyleneimine) polymer with the lowest concentration (0.1 wt%) would yield the highest SEY.

Table of Contents

| | |
|--|----|
| 1 Diamond..... | 1 |
| 1.0 General..... | 1 |
| 1.1 Diamond Doping..... | 3 |
| 1.2 Synthetic Diamond..... | 5 |
| 1.2.0 High Pressure, High Temperature (HPHT)..... | 5 |
| 1.2.1 Chemical Vapour Deposition (CVD)..... | 5 |
| 1.3 Diamond Surfaces..... | 9 |
| 1.4 Surface Termination..... | 9 |
| 2 Theory..... | 12 |
| 2.0 Band Theory..... | 12 |
| 2.1 Band Diagram..... | 13 |
| 2.2 Semiconductors..... | 13 |
| 2.2.0 Intrinsic Semiconductors..... | 13 |
| 2.2.1 Extrinsic Semiconductors..... | 13 |
| 2.3 Band Bending..... | 14 |
| 2.4 Electron Affinity..... | 15 |
| 2.5 Negative Electron Affinity (NEA)..... | 15 |
| 2.6 'True' and 'Effective' Negative Electron Affinity..... | 16 |
| 2.7 Secondary Electron Emission Yield (SEELY)..... | 17 |
| 3 Aims and Objectives..... | 19 |
| 4 Experimental..... | 20 |
| 4.0 Preliminary Tests..... | 20 |
| 4.0.0 Zeta Potential..... | 20 |

| | |
|---|----|
| 4.1 Sample preparation..... | 20 |
| 4.1.0 Techniques..... | 20 |
| 4.1.0.0 Cleaning..... | 20 |
| 4.1.0.1 Oxidation..... | 20 |
| 4.1.0.2 Sonication of Diamond Suspension..... | 20 |
| 4.1.0.3 Self-assembly of Diamond..... | 20 |
| 4.1.0.4 O,Li Functionalization Process..... | 21 |
| 4.1.0.4.0 Annealing..... | 21 |
| 4.1.0.4.1 O-Termination..... | 21 |
| 4.1.0.4.2 Lithiation..... | 21 |
| 4.1.1 Batch 1..... | 22 |
| 4.1.2 Batch 2..... | 22 |
| 4.1.3 Batch 3..... | 23 |
| 4.2 Sample Characterization Method..... | 23 |
| 4.2.0 Raman Spectroscopy..... | 23 |
| 4.2.1 Scanning Electron Microscopy..... | 24 |
| 4.2.2 Contact Angle..... | 24 |
| 4.2.3 Secondary Electron Emission Yield..... | 24 |
| 5 Results and Discussion..... | 27 |
| 5.0 Preliminary Tests..... | 27 |
| 5.0.0 Raman Spectroscopy..... | 27 |
| 5.0.1 Contact Angle Measurements..... | 28 |
| 5.0.2 Zeta Potential..... | 29 |
| 5.0.3 Scanning Electron Microscopy..... | 29 |

| | |
|--|----|
| 5.1 Batch 1..... | 30 |
| 5.1.0 Contact Angle Measurements..... | 30 |
| 5.1.1 Scanning Electron Microscopy..... | 31 |
| 5.1.2 Luminescence..... | 32 |
| 5.1.3 Secondary Electron Emission Yield..... | 33 |
| 5.2 Batch 2..... | 34 |
| 5.2.0 Contact Angle Measurements..... | 34 |
| 5.2.1 Scanning Electron Microscopy..... | 34 |
| 5.2.2 Luminescence..... | 35 |
| 5.2.3 Secondary Electron Emission Yield..... | 35 |
| 5.3 Batch 3..... | 35 |
| 5.3.0 Contact Angle Measurements..... | 35 |
| 5.3.1 Scanning Electron Microscopy..... | 36 |
| 5.3.2 Luminescence..... | 36 |
| 5.3.3 Secondary Electron Emission Yield..... | 36 |
| 6 Conclusion..... | 37 |
| 7 Further Work..... | 40 |
| 8 Reference..... | 41 |

1 Diamond

1.0 General

Diamond has been esteemed for its scarcity for centuries and remains standing as a symbol of eminence and fortune^[1]. It has been renowned as one of the most extraordinary materials of today, owing to its phenomenal physical properties, giving rise to a wealth of applications. Diamond comes from the Greek word, *adamas*, for unconquerable^[2] as demonstrated in its extreme hardness of *ca.* 90 GPa^[3]. It is optically transparent from the ultra-violet (UV) to the far infra-red (IR) region (>70% transmission for wavelengths greater than 1 μm)^[3]. The above physical properties of diamond are some of the few that make it an exceptional gemstone. Diamond's inertness to a vast majority of chemical reagents^[4,5] and its rigid structure^[1,5] enables it to be transformed into thin films of a few microns in depth, which may be employed in electronic applications^[4].

Natural diamonds have been formed in the Earth at great depths from carbonaceous material under high pressures and temperatures^[6]. Once formed, they are ejected with the parent rock in volcanic eruptions. These volcanic cones are comprised mainly of diamondiferous material and subsequent decay of the cones prompts diamond bearing material to be washed down the rivers. Consequently, alluvial deposits are formed^[7] and diamond is extractable. It was first discovered and mined in India several years ago, where considerable deposits of the stone were found in rivers^[2].

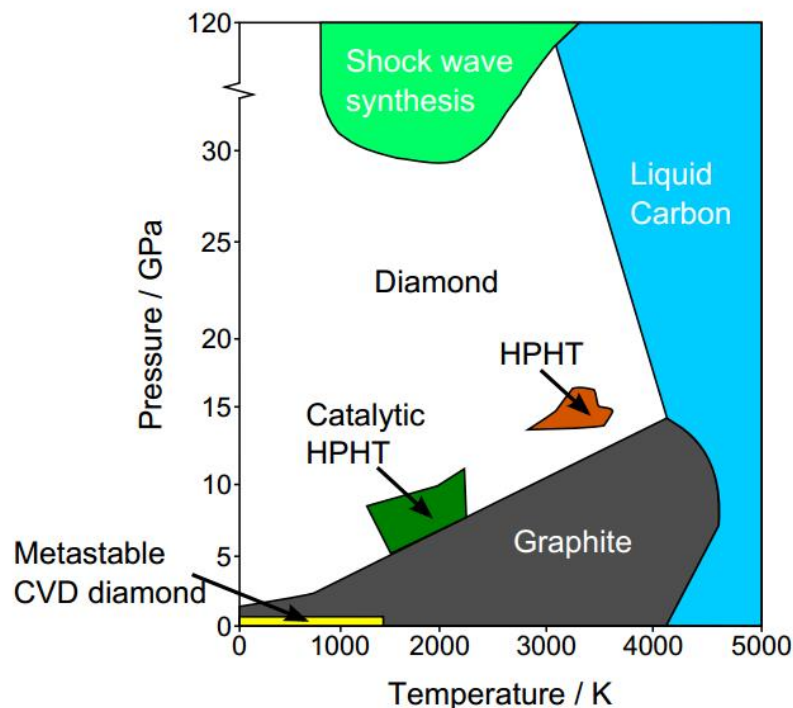


Figure 1.0: Pressure, temperature phase and reaction diagram of elemental Carbon from reference^[8].

There are numerous allotropes of carbon, attributable to its valency. The most common being graphite and diamond, whose relationship, when examining the phase diagram illustrated in figure 1.0, is both kinetic and thermodynamic. Their structures are depicted in figure 1.1. Other allotropes

include amorphous carbon and fullerenes (such as C₆₀). At room temperature and atmospheric pressure, graphite is the thermodynamically favoured allotrope demonstrated in figure 1.0. On the contrary, at higher temperatures and pressures, diamond exists as the most stable form. However, we can also see from figure 1.0 that diamond can exist at lower temperatures and pressures, like graphite. This is the result of the very large activation barrier for the conversion between the two allotropes. Thus, once formed, diamond is said to be metastable^[9], that is, kinetically stable but thermodynamically unstable.

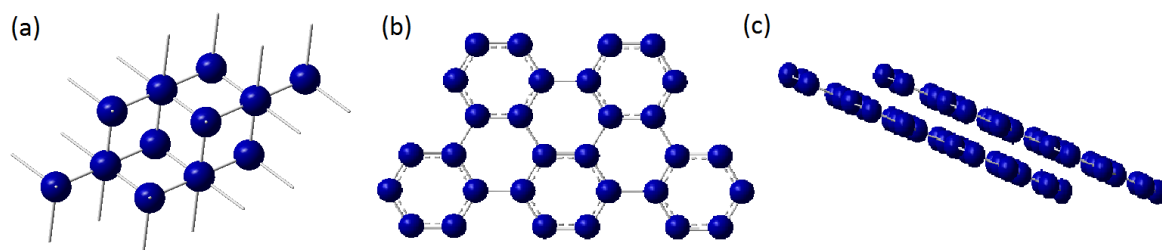


Figure 1.1: The two main allotropes of carbon, where (a) is diamond and (b) and (c) are graphite.

Carbon has a filled valence shell with the electronic configuration of $2s^2 2p^2$. Regarding diamond, these s and p orbitals hybridise to form sp^3 orbitals which accommodate a tetrahedral structure, with a C-C-C bond angle of 109.5° ^[10]. Strong covalent bonds are then formed in which the outer electrons of carbon are localised^[6]. These carbon atoms are arranged in a variation of the face-centred cubic, three-dimensional crystal lattice structure, depicted in (a) of figure 1.2. The sp^3 hybridised orbitals in diamond differentiate it from the other allotropes of carbon, which have sp^2 hybridisation, and gives diamond its unique and remarkable properties. In diamond and graphite (figure 1.1 (b) and (c)), the nearest neighbours are separated by a distance of 1.54 \AA and 1.42 \AA , respectively^[11]. The shorter bond lengths in graphite can be accounted for by the double bonds, found in graphite, having shorter distances than single bonds, found in diamond. This implies that graphite is stronger in plane than diamond, hence, there is interest in carbon nanotubes (graphite tubes) and graphene (single sheets) for 3-D and 2-D electronic applications^[12,13]. In graphite, the carbon atoms are organised in layers of interconnected hexagonal rings (figure 1.1(c)), separated by a distance of 3.41 \AA ^[14]. These layers are kept together by weak dispersion forces.

Diamond has a very high secondary electron yield and has valuable applications in devices, for instance, electron multipliers^[15]. The total electron yield as a function of incident electron energy and the energy distribution of the emitted secondary electrons has demonstrated that both bulk properties and surface chemistry play a vital role in the secondary electron emission process^[15]. This will be explained in more detail later. Metals and semiconductors are predominantly poor secondary electron emitters, whereas the opposite is true for insulators^[16]. Natural diamond exists as an electrical insulator with a resistivity of $10^{16} \text{ \Omega cm}$ at room temperature^[3] and a band gap of 5.45 eV at 300 K ^[17]. The lack of delocalised electrons in diamond explains the unattainable electrical conduction. It is necessary, however, for insulators to supply some level of electrical conductivity.

1.1 Diamond Doping

Diamond does not support a native oxide. For this reason, it is possible to functionalise it with various dopants^[18]. Doping diamond diminishes the band gap, thereby inducing electrical conductivity and forms an extrinsic semiconductor. The dopant type and dopant concentration influence the movement of secondary electrons through the sample bulk, as well as the electrical conductivity necessary to replenish the emitted electrons.

Doping techniques include: ion implantation^[19], introduction into the plasma during CVD growth^[20] and in-diffusion employing chemical dopants^[21]. Doping was first done by ion implantation at the end of the 1960s^[22], however, this approach caused irreversible damage to the crystal. In the 1980s, it became possible to add dopants to the gas phase during growth^[23].

Incorporation of impurities into the bulk of a diamond can enhance or diminish crystal properties and can create an effective negative electron affinity on the surface. This phenomenon will be explained later. Upon doping, metals, for instance, Fe, Co and Ni, diminish the properties of diamond, whereas O, N, Li, Na or B potentially enhance diamond's electrical properties^[24,25,26]. The latter dopants establish an energy level inside the band gap, decreasing the barrier to electrical conductivity, converting diamond from an insulator to a semiconductor^[27]. Figure 1.3 displays the band gap of intrinsic diamond, *p*-type diamond and *n*-type diamond. Intrinsic diamond has a larger activation energy, that is, the energy required for an electron to be promoted from the valence band maximum ($_{\max}E_v$) to the conduction band minimum ($_{\min}E_c$), of 5.45 eV as mentioned above. This value suggests that it is an electrical insulator.

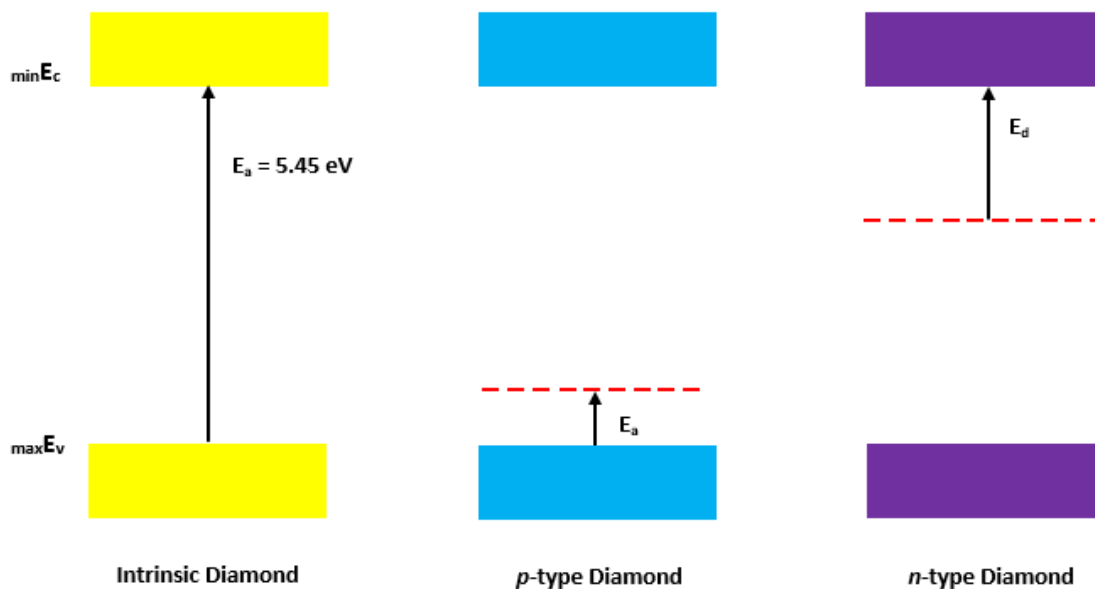


Figure 1.3: Band diagram of intrinsic diamond, *p*-type diamond and *n*-type diamond. Inspired by^[28].

p-type diamond has an acceptor energy level close to the valence band maximum^[28]. This causes electron holes to shift from the valence band to the acceptor band. An acceptor generally has one electron fewer than carbon and normally has the ability to substitute for a carbon atom in a diamond lattice. As a consequence to the deficient electron, the dopant will create a free, positively charged hole which is electrically conducting upon accepting an electron from the neighbouring carbon. Thus, a *p*-type dopant is referred to as an acceptor. *n*-type dopants, on the other hand, can be any element which has a greater number of electrons than carbon, and, similar to *p*-type dopants, has the capacity to substitute for a carbon atom in the diamond lattice. Here, electron movement occurs from the donor band to the conduction band. The *n*-type energy level represented in figure 1.3 is close to the conduction band minimum, where the spare electron will be incorporated, hence changing the electrical properties of the diamond.

There are two types of donor/acceptor levels: 'shallow' and 'deep'. The former arises from dopants being in close proximity to either end of the band gap. Thus, inducing a low activation energy. The latter, however, is found mid-band gap and has a larger activation energy. Consequently, *p*-type dopants have 'shallow' acceptor levels with low activation energies, whereas *n*-type dopants have 'deep' donor levels with high activation energies.

Lithium is an element which is capable of integrating into the diamond lattice interstitially and has been recognised as a possible *n*-type dopant. Current DFT results^[29] have confirmed lithium's shallow *n*-type nature when filling tetrahedral interstitial sites in diamond with a formation energy of 8.2 eV^[30]. The lowest energy position has T_d symmetry with lengthened C-C bonds. In contrast to theoretical calculations, experimental results have indicated that both lithium and sodium doped diamonds are electrical insulators^[31,32]. This could be accounted for by the good mobility of lithium in a diamond lattice; the diffusion activation energy has been evaluated at 0.26 eV^[31]. The mobility stimulates the diffusion of lithium donors at vacancies in the diamond which effectively cancel the electron-donating donors produced by Li in the interstitial T_d positions. This results in substitutional lithium atoms with a subsequent formation energy of 4.12 eV^[29].

Numerous techniques of lithium doping exist. One method has been undertaken by Dr. Neil Fox, Department of Physics, University of Bristol, which involves the mixing and annealing of diamond and lithium carbide. This induces diffusion of lithium into the diamond, or deposition of a diamond film by CVD onto a substrate seeded with lithiated diamond nanoparticles^[33]. Thermal annealing is a useful heat treatment which has the ability to alter a diamond's properties. It regenerates the diamond lattice and removes any impurities. In the case of lithium, once annealed, lithium-doped diamond will display *n*-type behaviour^[34]. Research has been done which examined the surface conductivity of H-terminated diamond after thermal annealing in vacuum^[35]. It was found that after the heat treatment at temperatures below 190°, surface conductivity is recovered.

Today, boron is the most accustomed dopant to produce conducting diamond electrodes^[36] and results in a *p*-type semiconductor^[37,38]. This is attributed to the low charge carrier activation energy of 0.37 eV^[36], seen in figure 1.4. Other dopants include: phosphorous, with a charge carrier activation energy of 0.6 eV^[39,40] and nitrogen, with a charge carrier activation energy of 1.6-1.7 eV^[40]. Phosphorous and nitrogen doped diamonds produce *n*-type semiconductors^[38,39,40]. Boron doped diamond surfaces produce a narrow energy distribution of low-energy secondary emission^[41].

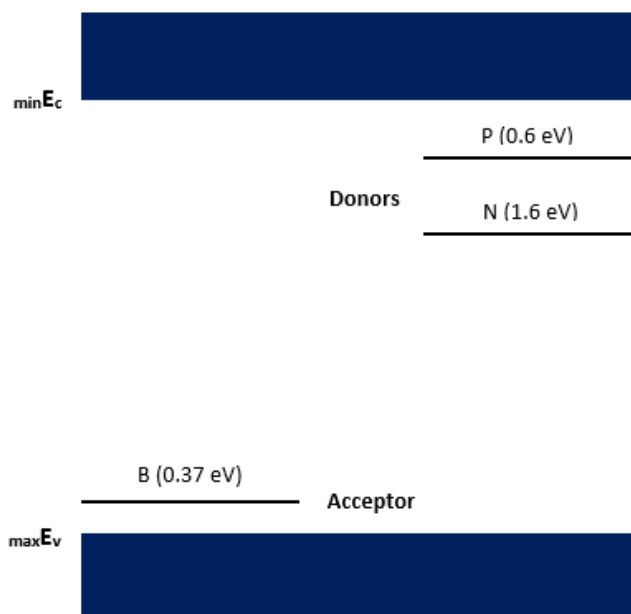


Figure 1.4: Different dopants and their charge carrier activation energies.

1.2 Synthetic Diamond

There are two methods of growing diamond: High Pressure, High Temperature (HPHT) and Chemical Vapour Deposition (CVD). These will be discussed in the following section.

1.2.0 High Pressure, High Temperature (HPHT)

Diamond is the most dense allotrope of carbon ($\rho_{\text{diamond}} = 3513 \text{ kgm}^{-3}$, $\rho_{\text{graphite}} = 226 \text{ kgm}^{-3}$ at 293 K)^[42]. Consequently, at high pressure, diamond must be the stable form of solid carbon, as mentioned above. This is the underlying idea behind the HPHT method.

Artificial diamond was first successfully synthesized in the 1950s using the HPHT technique^[43]. The process essentially mimics the conditions under which natural diamond forms deep in the Earth. Graphite is constricted to hydraulic pressure of thousands of atmospheres, heated to over 2000 K in the presence of a suitable metal catalyst and left until diamond crystallises^[1].

The pitfall of this technique is that it produces diamond as single crystals which vary in size from 2.5 nm to 3.2 mm^[44]. This restriction affects the variety of applications for which it can be used. HPHT diamond also has a very limited shape. This is a consequence of it being an economical process. An alternative method was therefore discovered; CVD.

1.2.1 Chemical Vapour Deposition (CVD)

Contrary to other high band-gap materials (e.g. AlN), synthetic CVD diamond is simple to produce. The important development arose in the 1960s, when Angus's group detected the presence of H atoms during the deposition process and determined its importance in the preferential etching of the graphite over diamond^[45].

CVD, as the name suggests, relates to a gas phase chemical reaction occurring above a solid surface, the substrate, which stimulates deposition onto that surface^[42]. CVD is currently an area of active global research^[46,47].

Unlike HPHT diamond, it is feasible to grow CVD diamond under conditions of high purity, ensuring minor defects^[48]. Other advantages include the prospect of growing diamond over substantial areas and the ability to control the properties of the diamond produced. This introduces many of diamonds principal qualities to other materials. For example, coated valve rings or cutting tools profit from diamonds hardness and wear resistance^[1]. On ample heat producing components, a diamond coating operates as a heat sink^[49]. CVD diamond coatings have also been grown uniformly on the surface of metallic wires or ceramic fibres^[50].

The growth of diamond via the CVD technique can be divided up into three stages; firstly, the activation of the gas mixture into their relative fragments; secondly, the gas-phase reactions of these fragments, and finally, the gas-surface and surface reactions which integrate these species into the bulk diamond.

The first step involves mixing the precursor gases in the chamber at *ca.* 800 °C and <10 kPa^[5]. These process gases comprise mostly of molecular hydrogen, but occasionally argon (*ca.* 10 %) and a carbon source, such as methane (*ca.* 5 %)^[48]. In the chamber, a substrate, in which diamond will grow, is deposited. The gases diffuse towards the substrate surface.

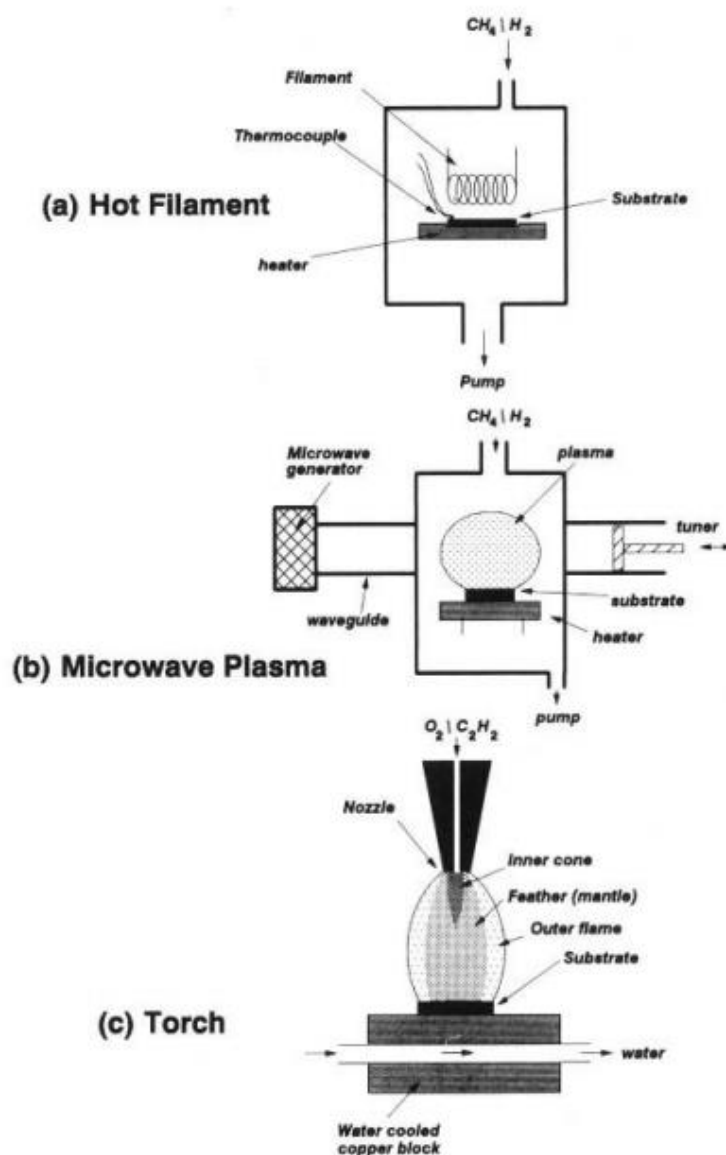


Figure 1.5: Schematic diagram showing three of the most frequently used types of diamond CVD apparatus. (a) Hot Filament reactor, (b) Microwave Plasma Enhanced CVD reactor, and (c) Oxyacetylene Torch. Adapted from^[42].

The second step necessitates a mode of activating gas-phase carbon-containing precursor molecules. The three customary methods used are hot filament activation (thermal method), microwave plasma (electrical discharge) and an oxyacetylene torch (combustion flame)^[42,51], the schematic drawings of which are presented in figure 1.5. All of these techniques vary in specific ways. For example, the precursor gas, routinely methane, has to be diluted in excess hydrogen, in a characteristic ratio of 1-5 %^[52]. In addition, the temperature of the sample is typically $>700\text{ }^\circ\text{C}$ to establish the presence of diamond over amorphous carbon^[1]. In each activation region, the molecules are energised which causes them to dissociate into reactive fragments, including a large number of hydrogen atoms. The high concentration of hydrogen leads to H-shifting reactions^[51], driving the whole chemical system, where the reactive fragments maintain mixing and undergo a complete set of chemical reactions. For example, the dissociation of molecular hydrogen to atomic

hydrogen, as either a hot filament process (equation 1.0) or microwave plasma method (equation 1.1)^[53].



The final step is the reaction of the gas-phase species with the substrate, and eventually their incorporation into the bulk diamond. The outcome is that both diamond and graphite grow on the substrate and in most cases, with a hydrogen terminated surface, due to the presence of excess hydrogen just above the substrate.

Over the past few decades, there have been numerous studies^[54] on the gas-phase chemistry involved in the CVD process. Now, all the components of CVD growth, C, H and O gases, can be summarized into a C-H-O phase diagram, referred to as the *Bachmann Triangle*, figure 1.6, and was pioneered by Bachmann *et. al.* in 1994^[55]. This phase diagram assists a comprehensive understanding of the key processes involved. It is comprised of three segments: non-diamond carbon, diamond growth region and no growth. Bachmann recognised that diamond would only grow when the gas mixture was adjacent to and just beyond the CO-tie line, thus deducing that diamond deposition was, essentially, independent of the nature of the course gases, but dependant of the C, H and O ratio.

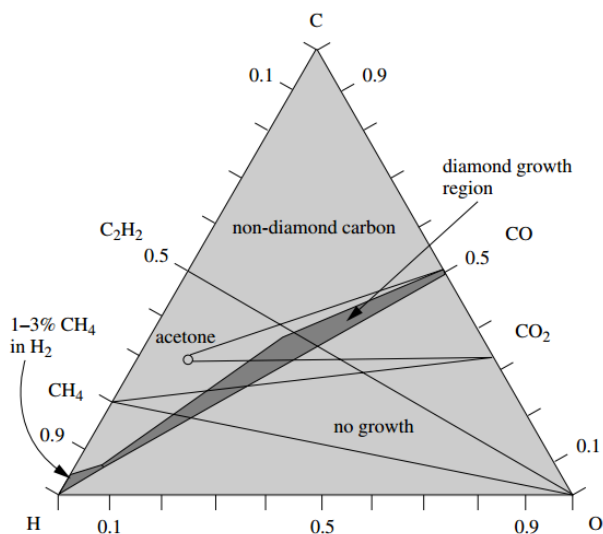


Figure 1.6: A simplified atomic C-H-O diamond deposition phase diagram: *Bachmann Triangle*, from^[1]. Beneath the CO-tie line exists no diamond deposition. Above the CO-tie line, non-diamond carbon is produced. In close proximity to and just above the CO-tie line, diamond is successfully deposited.

1.3 Diamond Surfaces

There are three primary planes which dominate on diamond surfaces: the [100] plane, the [110] plane and the [111] plane, presented in figure 1.7. These fundamental crystallographic orientations have their own unique properties. They all contain dangling bonds which form π -electron systems. The [100] face has two dangling bonds per surface atom, whereas the [110] and [111] faces have one. These result in different densities of surface states based on the shapes of the surfaces and have the ability to alter the electron affinity properties of the surface.

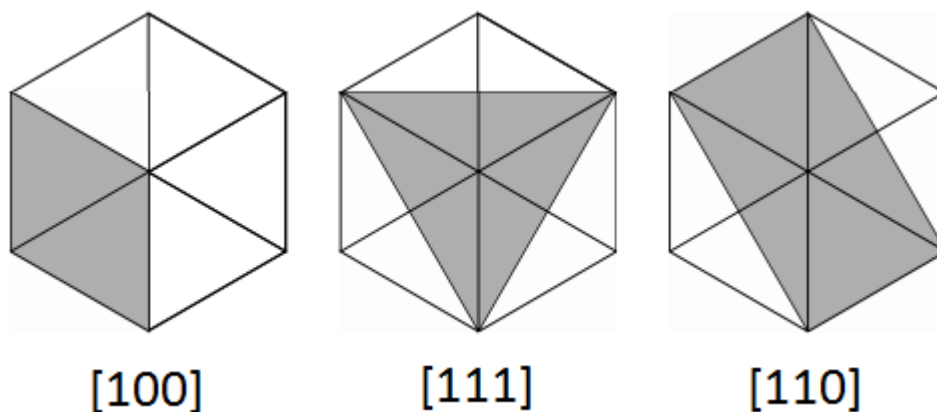


Figure 1.7: planes [100], [111] and [110] from an arbitrary unit cell^[56].

The theoretical strength of diamond has been evaluated for the three surface planes, deducing that it is heavily determined by crystallographic orientation^[57]. The [111] plane is the natural cleavage plane for a break in the crystal diamond on account of its low bond density^[57]. The tensile strengths increase from the [111] face to the [100] face.

CVD growth on the [100] diamond forms a cubic morphology which is remarkably even^[53]. [100] diamonds tend to have fewer defects in comparison to other planes^[53], making it a key focal point in experimental and theoretical studies^[58]. Diamond growth on the [111] plane is a rapid yet complex process. Due to the nature of this face, it is prone to defects as well as insertion of sizeable heteroatom species^[53]. The [100] and [111] faces require the longest time to grow^[59]. The [110] plane, on the other hand, is the fastest growing diamond surface^[53].

1.4 Surface Termination

A number of diamonds electronic properties occur as a result of a dipole, which in turn is brought about by the termination of the dangling sp^3 bonds on the surface by any species with the exception of carbon, figure 1.8. This modification of the surface chemistry largely influences the changes in the electronic properties. This adsorption gives rise to chemisorbed species and is named surface termination. Without termination, the diamond surface consists of dangling bonds which gives the surface a positive electron affinity and the diamond insulating properties. Additionally, cross-linkage will occur generating sp^2 graphitization^[15].

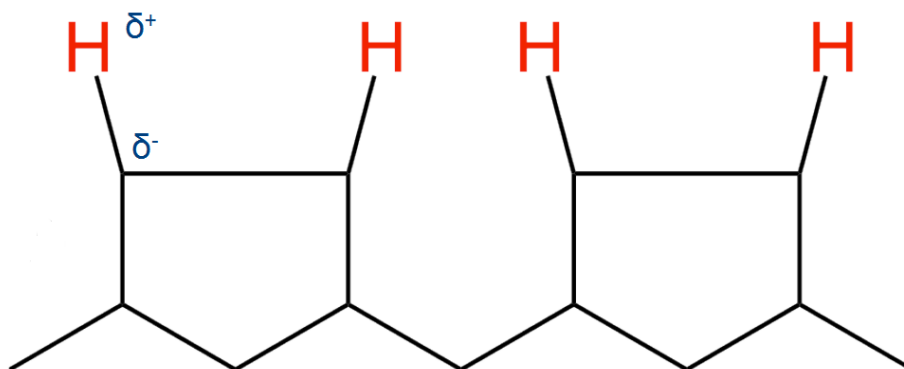


Figure 1.8: The dangling bonds on the surface of H-terminated C(100)-(2x1) diamond surface. The electronegativity differences of H and C of 2.20 and 2.55^[60], respectively, induce a dipole on the surface where the electrons from the bulk are attracted to and, thus, are emitted into the vacuum more efficiently.

Electronically, the most stimulating termination species are hydrogen, oxygen and combination species, such as $-\text{OH}$. For clarity, it is important to note that electronically, there are differences in the properties in the bulk and at the surface of the diamond owing to the electrons density distinction between the two.

Aforementioned, with respect to diamond, hydrogen atoms are a vital substituent in surface reactions, as we have previously seen. They create and re-terminate the reactive surface sites required for the propagation of the lattice^[61]. This hydrogenation yields a chemically inert H-termination layer. Previous studies^[62,63] have demonstrated that the majority of natural diamonds and CVD diamond films are H-terminated. Moreover, studies on the photoemission of the [111] surface of a single crystal diamond^[64] and emission testing^[65] have shown that H-termination was accountable for the negative electron affinity (NEA) properties, where the conduction band is higher in energy than the vacuum level. The NEA values range from -1.1 eV ^[63] to -1.3 eV ^[67]. This NEA effect enhances the secondary electron emission yield, the reason for which will be explained later. A recent study by O. A. Williams and R. B. Jackman^[68] showed that a large presence of chemisorbed hydrogen atoms on the surface of diamond is essential for the high surface conductivity.

H-termination also has the ability to stabilize the diamond lattice^[15]. The H-terminated surface is stable at high temperatures reaching $900 \text{ }^\circ\text{C}$ ^[69] on account of the high C-H bond energy of 4.2 eV ^[70]. Hydrogen has low electronegativity and it has been reported that as a result of this difference in dipole on the surface of diamond, depicted in figure 1.7, emission currents increase and threshold voltages decrease^[71].

One method for the preparation of a H-terminated surface uses a hydrogen plasma at $400 \text{ }^\circ\text{C}$ ^[72], which produces microscopic inhomogeneities at the surface which are due to a 1 nm layer of non-diamond material. This displays notable improvement in the electron emission properties. H-terminated diamonds have demonstrated shallow p -type levels. This extends 30 nm into the

surface^[73] where valence band electrons go. Left behind are positively charged cavities in the valence band which results in surface conductivity. These cavities assemble, the Fermi level drops, the work function expands and a large barrier to electron emission arises.

On the contrary to H-termination, oxygen terminated diamond displays insulating properties at the surface^[35] and a positive electron affinity. One study concerning the electrochemical properties of as-deposited and oxygen-treated polycrystalline diamond films have been reported^[74]. The oxygen termination lowered the energy matching possibility of the diamond-valence-band-edge with other redox couples. This in turn inhibited the electron transfer and, hence, conductivity dramatically decreased.

Electronically, hydrogenated surfaces display NEA properties while oxygenated surfaces display the opposite. -OH terminated surfaces, however, demonstrate a small NEA^[75].

Other properties of diamond can determine whether the surface is H- or O- terminated, such as, wetting capabilities^[76] and optical characteristics^[77].

2 Theory

2.0 Band Theory

Bonding in metals can be accounted for using band theory^[78] which is an adapted model of molecular orbital theory. In basic terms, atoms react to produce compounds. Their atomic orbital energies come together and produce molecular orbital energies. On an infinite scale, many of these energy levels will be proximate and, at times, degenerate, in energy. This enables the ‘tight-binding-approximation’, where the energy levels have formed bands of energy.

The ‘tight-binding-approximation’ states that electrons occupying a partially filled band are able to freely populate the accessible energy levels, thus, inducing electrical conduction. Here, the electrons act as free charge carriers. As mentioned above, energy bands arise as a consequence of infinite molecular orbital energies being in close proximity, or even degenerate. There exists a huge variety of possibilities, consequently, bands with diverse energies and band gaps are established, demonstrated in figure 2.0.

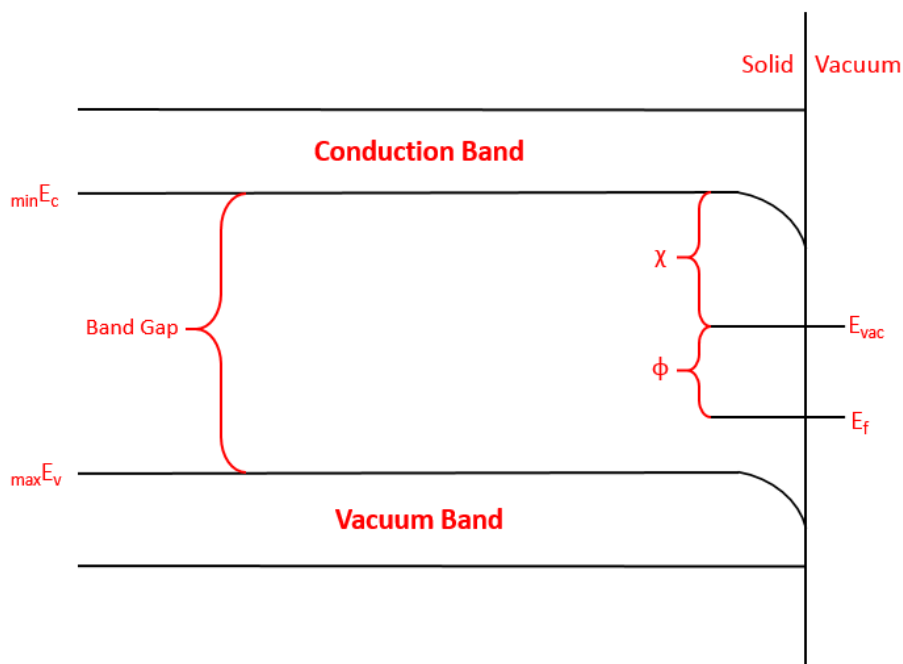


Figure 2.0: A band diagram of a *p*-type semiconductor, showing the conduction band minimum ($min E_c$), the valence band maximum ($max E_v$), the vacuum level (E_{vac}), the Fermi level (E_f), the electron affinity (χ) and the work function (ϕ), inspired by^[79].

Band theory can estimate possible metallic characteristics of a material. It studies the ‘jump’ of electrons over the band gap, past the Fermi level. This gives information about the optical and magnetic properties^[80] of the material, while also assisting in the theory behind semiconductors and doping^[80].

2.1 Band Diagram

Band diagrams are a means of illustrating band theory. The band diagram of diamond was initially pioneered in the 1970s using Ab Initio techniques^[81]. Band diagrams demonstrate the band structure of filled and unfilled molecular orbitals within the valence band, seen in figure 2.0. In the former case, the electrons are localised in the band and movement is restricted. Despite this, electrical conduction can be achieved if the conduction band is close enough to the valence band, accommodating the promotion of electrons. This results in these bands being partially occupied. Here, we assume that the mobile negative charge is the electron movement and that this movement from the valence band to the conduction band results in the formation of positive cavities. So, these positive cavities are attributed to the electron deficiency. Both, the electrons and positive cavities are correspondingly mobile and are able to transfer charge.

The band gap is the product of the difference between the conduction band minimum, $_{\min}E_c$, and the valence band maximum, $_{\max}E_v$. The conduction band minimum is evaluated by normalising the negative electron affinity peak on the normal emission spectra fabricated in 1998^[82].

The highest occupied molecular orbital at absolute zero is assigned the Fermi level, E_f . It is generally situated amidst the conduction band minimum and the valence band maximum. The electrons at the Fermi level have their independent quantum states, which, with increasing temperature, start to occupy states beyond the Fermi level, leaving the states below unoccupied. The value of the Fermi level is employed in the determination of the work function, ϕ , and is established by the energy difference between the vacuum level, E_{vac} , and the Fermi level. At the vacuum level, the electrons are not restricted to the surface of the material and hence are free to enter the vacuum. The Fermi level is dictated by the amount of doping in the bulk^[83].

2.2 Semiconductors

Semiconductors are characterised by their small band gap between the conduction band minimum and the valence band maximum. As stated in band theory, semiconductors behave as insulators at absolute zero. Above this temperature, however, the electrons have enough energy to overcome this barrier and the material is semiconducting in nature. In order for a material to be a semiconductor, it must have a fully occupied valence band and an unoccupied conduction band.

2.2.0 Intrinsic Semiconductors

These materials display semiconducting properties. The number of electrons in the conduction band is equivalent to the number of holes in the valence band. These semiconductors contain no impurities, so the energy required to excite an electron into the conduction band corresponds to the band gap. This can be achieved by thermal excitation, increasing the movement of electrons and results in an increase in electrical conduction.

2.2.1 Extrinsic Semiconductors

Extrinsic semiconductors have differing band structures subject to their properties and how they achieve their conductivity. They have been 'doped' using a variety of methods by small amounts of a

chemical to enhance electrical conductivity. The dopant achieves this by establishing one of two types of orbitals into the band structure: donor or acceptor orbitals. These dopants give rise to *n*-type and *p*-type semiconductors, illustrated in figure 2.1. The main difference between the two is the position of the Fermi level. The former has the Fermi level just above the valence band maximum, whereas the latter has the Fermi level just below the conduction band minimum. In the example given in figure 2.0, the vacuum level, lies somewhere below the conduction band. Accordingly, electrons moving into the conduction band have a negligible barrier to emission. This is a surface property and is labelled as the ‘effective’ negative electron affinity of a solid, which will be discussed later. In some cases, the vacuum level is found above the conduction band. Here, the energy required for the electrons to be emitted onto the surface is too high and the solid has a positive negative electron affinity.

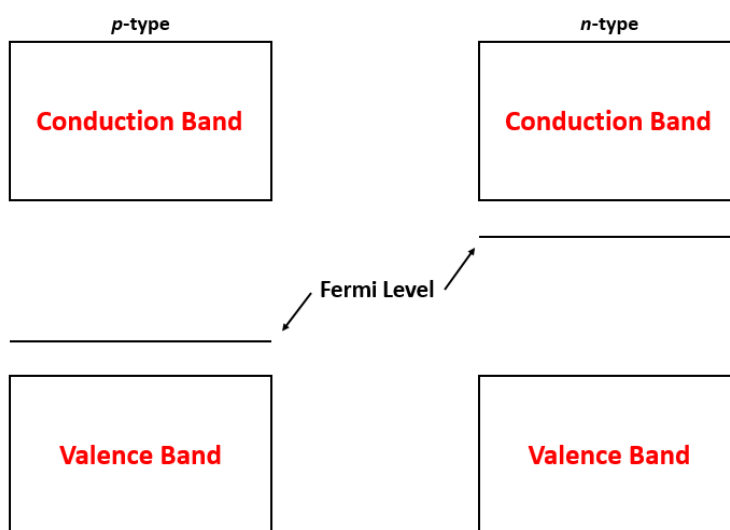


Figure 2.1: diagram illustrates *p*-type and *n*-type semiconductors and their relative Fermi levels, inspired by^[84].

2.3 Band Bending

There is a difference in the energy of electrons in the bulk of a material and on the surface, leading to band bending. It occurs just below the surface at the conduction band minimum and highlights the difference in the position of the conduction band at the surface and the bulk. This incident occurs due to the movements between these two sites^[85]. There are two types of band bending, upward and downward. Figure 2.0 is an example of downward band bending. *n*-type semiconductors normally have upward band bending, as a consequence of the electron movement from the bulk of the donor atom to the vacant surface. *p*-type semiconductors, on the other hand, as demonstrated in the figure, results in electron movement from the surface to the bulk of a material containing acceptor orbitals, thus, display downward band bending.

2.4 Electron affinity

Electron affinity is describe as the total energy release as an electron is added to an uncharged, gaseous species, producing a negatively charged, gaseous ion^[86], depicted in the below equation.



In terms of band theory, the electron affinity, χ , is the energy between the conduction band minimum and the vacuum level. This energy is the energy required for an electron in the conduction band to leak into the vacuum. It is also possible for an insulator to release these electrons, but they are not the electrons required for conduction. Semiconductors, on the other hand, can supply such electrons which constantly replenish surface conductivity. Hence, semiconductors are ideal for electron emitting applications^[87].

2.5 Negative electron affinity

The barrier to emission experienced by electrons in the conduction band prevents them from spontaneously entering the vacuum. This barrier arises when the vacuum level, is higher than the conduction band, giving rise to a positive electron affinity (PEA), displayed in figure 2.2. This consequently lowers the number of electrons emitted into the vacuum as they are harder to remove.

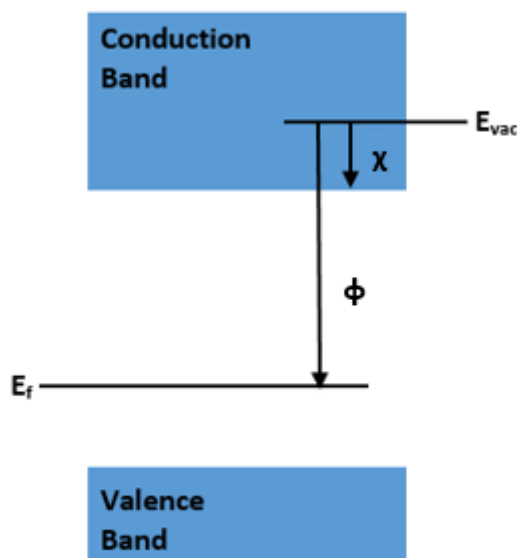


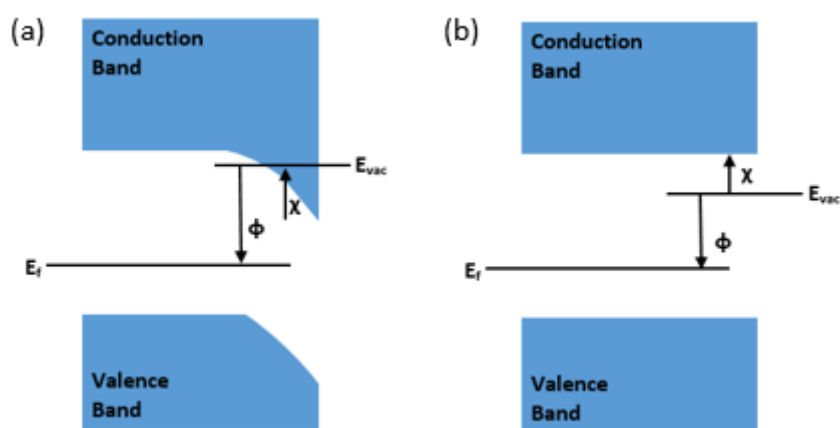
Figure 2.2: Energy band diagram of a positive electron affinity (PEA) surface.

Occasionally, the conduction band is raised, so that the vacuum level is below the conduction band level. Here, the electrons can be emitted from the surface to the vacuum, resulting in a negative electron affinity (NEA). Obtaining an NEA surface has been a focal point in research, as the barrier is significantly diminished, generating spontaneous emission of a thermalized electron^[85] and can be obtained through doping or surface termination^[88].

Several diamond surfaces display an NEA making them good field emitters^[89,90]. The majority of surfaces, however, have a PEA, demonstrated on bare, undoped, unterminated diamond and oxygen-terminated diamond. If a positive surface charge is generated, with respect to the bulk, a net attraction to the surface arises, reducing the barrier to emission, obtaining an NEA. Materials which exhibit such electrical properties have a larger secondary electron emission yield.

2.6 'True' and 'Effective' Negative Electron Affinity

A paper published in 1996^[91] established two main NEA subcategories; the 'effective' and 'true' NEA. These are illustrated in figures 2.3(a) and 2.3(b), respectively.



Figures 2.3: Vacuum level, E_{vac} , lying below the conduction band, indicative of (a) an effective negative electron affinity surface, and (b) a 'true' negative electron affinity surface.

'True' NEA is a product of polarity differences in the bulk and surface of a material. This dipole is able to 'pull' the vacuum level under the conduction band level^[92,93,94,95]. An example of this is in H-terminated diamond surfaces^[92,93,95,96,97,98], which is generated by the difference in electronegativity between carbon and hydrogen as mentioned above. This suggests that the H atom acquires a positive charge in relation to the carbon atom, producing a dipole, as mentioned previously in figure 1.7. In figure 2.3(b), there is an upward transfer in the bands at the surface, reducing the work function and ensuring that the vacuum level is below the conduction band. The electrons are then discharged from the conduction band into the vacuum.

Band bending means that the result is the same for the 'effective' NEA case. This type of NEA has the vacuum level below the conduction band bulk, but as the conduction band bends, the conduction band minimum is found below it. This enables non-thermalised electrons to be emitted into the vacuum.

2.7 Secondary electron emission

Three forms of electron emission from a solid surface exist; thermionic emission, field emission and secondary electron emission. Thermionic emission is the heat induced flow of electrons from a surface. The thermal energy supplied is large enough to overcome the work function. It was first reported in 1873 by Guthrie^[99]. The second form of electron emission is field emission. These electrons are induced by an electrostatic field. It was described by quantum-mechanical tunnelling of the electrons in 1928 by Fowler and Nordheim^[100]. The third, and most important for the purpose of this thesis, is secondary electron emission. It is an important subject of present day research^[101,102]. It is the emission of secondary electrons from a surface as the primary incident electrons with sufficient energy attack^[96]. The mechanism of which is depicted in figure 2.4. It is possible to modify a diamond surface so that when an electron is irradiated, at least one electron can be released from the surface. Diamond, therefore, has the potential to yield very high secondary electron emission. UV photoemission data has shown that diamond has a sharp, intense peak at *ca.* 5 eV with a narrow linewidth, typical of a negative electron affinity surface. This leads to the excitation of electrons straight from the conduction band minimum of diamond^[64,89,92,101,102]. This can also be true for positive electron affinity surfaces^[105].

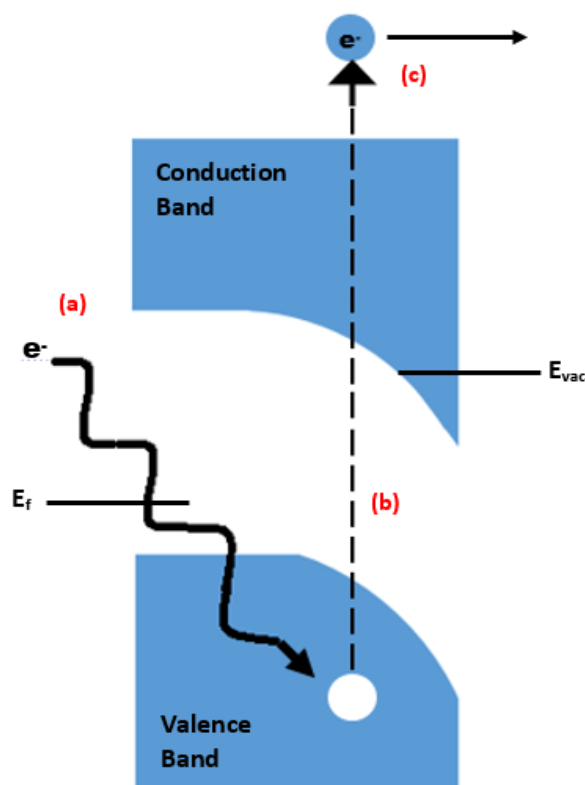


Figure 2.4: Mechanism proceeds as follows: (a) the primary electron penetrates the surface of the material, generating a secondary electron, (b) this secondary electron then undergoes a number of collision, resulting in a loss of energy greater than the band gap. The final step, (c), sees the secondary electron escaping into the vacuum.

As an electron beam with an energy, E_p , is incident on a solid surface, scattering occurs into the vacuum via elastic or inelastic scattering^[106]. Inelastic scattering produces secondary electrons which have experienced a number of collisions, resulting in a loss of energy greater than the band gap, hence, exciting the secondary electrons from the valence band to the conduction band. This is depicted in secondary electron energy distribution curves^[107].

In the 1930s, it was thought that photoemission was a surface effect instead of a bulk effect^[108]. Today, it is recognised that the primary electrons penetrate the material, so secondary electrons are transmitted throughout the bulk, leading to their emission. Research done in the 1990s suggested that there was a direct link between the energy of the incident electrons and the secondary electron emission yield^[109]. This is partially true as the penetration depth of the primary electron and the escape depth of the secondary electron must be considered too.

The mechanism of secondary electron emission had been reported in various ways. Spicer developed a Three-Step model^[110], which divides photoemission into three successive steps: optical absorption, electron transport and escape through the surface, illustrated in figure 2.4. The first step encompasses the excitation of electrons from the valence band after absorption of energy. The second step, as the name implies, is the movement of the electrons through the bulk of the material and onto the surface. In the final step, the electrons are emitted from the surface into the vacuum^[109]. The Three-Step model is widely used in the theory behind research^[112,113,114]. Another study, by Pate *et. al.*^[115] outlines two possible routes for electrons upon excitation from a primary electron. These incident electrons lose energy by forming electron-hole pairs which are a product of excitation from the valence band maximum to the conduction band minimum, leaving behind a positively charged hole. They are held here by electrostatic Coulombic attraction, forming an exciton. These electrons now have two potential paths. The first is to fall back into the valence band and couple with the associated positive hole; exciton decay. The second is to vacate the conduction band and enter the vacuum; exciton dissociation. The excitons have an attraction towards the dipole present at the surface-vacuum interface and secondary electron emission is attributed to the break up of the bulk electrons^[84,115]. Secondary electron emission yield can multiply when secondary electrons collide with other electrons, creating more electron-hole pairs which build up in the conduction band^[111, 112].

3 Aims and Objectives

The aim of this project was to optimize the secondary electron emission yield of various diamond self-assembly samples, with particular emphasis on varying the metal and its oxidation times as well as the polymer.

Beryllium copper (BeCu), silver (Ag) and nickel (Ni) were the three metals used as substrates. The composition of the alloy, BeCu, was 98.0 % and 2 % of Cu and Be, respectively. BeCu has been used in electron multiplier devices as dynodes and yields very high secondary electron emission^[117,118,119]. Ag has been widely used in electronics and has also been shown to yield a high secondary electron emission^[119]. Similarly, Ni containing materials have formed the basis of some fundamental components in the electronics industry and has demonstrated good secondary electron emission^[120]. One objective of this project was to deduce which metal substrate yields the highest secondary electron emission yield and with which optimum oxidation time.

From section 1.4, the formation of a dipole on the surface of diamond is critical for the generation of a negative electron affinity surface. Thus, each sample was O-terminated and lithiated prior to self-assembly with the polymer and the diamond, which has previously demonstrated high secondary electron emission yields^[121].

The diamond used in this project was Monocrystalline Diamond Powder, MSY 0.4-0.6 micron dispersed in water. Water was chosen on account of its small surface charge on the nanodiamond which interacts with the dipole in water^[122]. This generated a stable diamond suspension. The zeta potential was discovered to be -35 mV, this process will be explained in section 4.0.1. Another objective for this project was to achieve a self-assembly; the oxidised metal substrates and the negative diamond potential required a positive layer between them. Two cationic polymers were used for this purpose: carboxyethyl silanetriol sodium salt (25 wt% in water) and poly(ethyleneimine) (50 wt% in water), their structures are shown in figure 3.0. The final objective for this project was to determine which of these polymers, essentially, acts as the best 'glue' and which concentration of that polymer is the optimum.

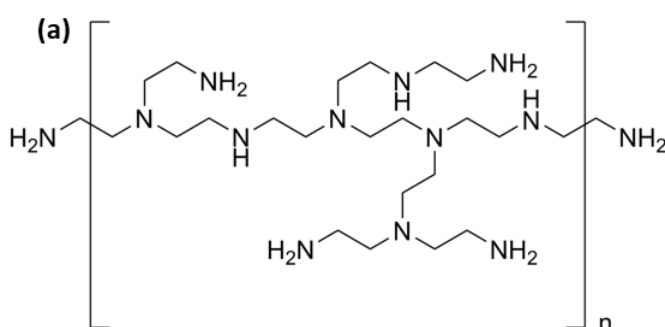


Figure 3.0(a): Poly(ethyleneimine)
50 wt% in water. $M_w \sim 750,000$

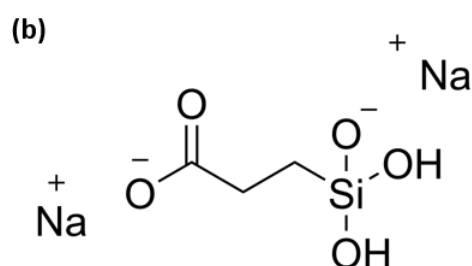


Figure 3.0(b): Carboxyethyl silanetriol
sodium salt 25 wt% in water. $M_w \sim 196.14$

4 Experimental

4.0 Preliminary Tests

4.0.0 Zeta Potential

Zeta Potential is used to determine the electrokinetic potential in colloidal systems. It is the electric potential in the interfacial double layer, i.e. between the bulk aqueous medium and the diamond-water interface^[123]. The result obtained reflects the charge on the diamond surface. Additionally, values between ± 30 mV and above suggest high colloidal stability.

Method: Nano Series Zetasizer, ZEN 2600 (Malvern U.K.) was used to analyse the zeta potential of the aqueous diamond suspension, which had been sonicated for 4 hours, at 25.1 °C.

4.1 Sample Preparation

4.1.0 Techniques

4.1.0.0 Cleaning

All the metal substrates were cleaned with ethanol, methanol and acetone to ensure no impurities were present on the surface.

4.1.0.1 Oxidation

The ultra-violet ozone (UVO) treatment had a suitable energy, 254 nm wavelengths^[124], to dissociate the ozone gas. These radical oxygen atoms were then deposited onto the metal substrate, which created an oxygen layer on the surface.

Method: Clean samples were positioned inside the Jetlight Co. Inc. UVO cleaner (model number: 42A-220) at room temperature for various times.

4.1.0.2 Sonication of Diamond Suspension

Upon sonication, particles are treated with sound energy, perturbing them. A study done at the University of Bristol^[27], highlighted the importance of sonication. An increase in uniformity was observed as the sonication time increased. This study concluded that sonication for 4 hours was the optimum and revealed an almost perfect distribution of the deposited diamond, whereas, sonication for shorter times displayed aggregates and mediocre distribution.

Method: An ultrasonic bath at ~80 Watts was used to break up the diamond aggregates, creating a uniform solution. All the experiments deducted in this thesis used a diamond suspension which had been sonicated for 4 hours.

4.1.0.3 Self-Assembly of Diamond

Self-assembly is a recent development in which diamond is seeded on top of a substrate. It employs the zeta potential charge of each layer, hence, relies on electrostatic attractions^[125] for stability.

Polymers are used as a positively charged layer and for their ability to construct an evenly-distributed, fully-coated surface.

4.1.0.4 O,Li Functionalization process

4.1.0.4.0 Annealing

The process of annealing is capable of altering the physical and chemical properties of a material. It involves heating a material to above its glass transition state and allowing it to cool. It refines structure making it homogeneous. It also increases the rate of diffusion of the material.

All the samples were heated to 450 °C and allowed to cool to room temperature using the Balzer 510 coating machine, situated in the Department of Physics, University of Bristol, the schematic diagram of which is depicted in figure 4.0.

4.1.0.4.1 O-termination

Using the Balzer 510 coating machine, the surface of the samples were O-terminated. This process was done under 0.03 Torr using Ar-O₂ at 20 % with 150 Watt power for 10 minutes. The samples reached 90 °C.

4.1.0.4.2 Lithiation

Using the same Balzer process, ≤ 15 nm of lithium metal was deposited onto the surface of the samples using an inverted tungsten boat source. The lithium deposition process was performed in the same pump-cycle as the anneal process and the O plasma treatment, shown in figure 4.0.

A study was done, which looked at the advantages of LiO-terminated diamond surfaces^[126], and concluded that this functionalization yields a high secondary electron emission yield.

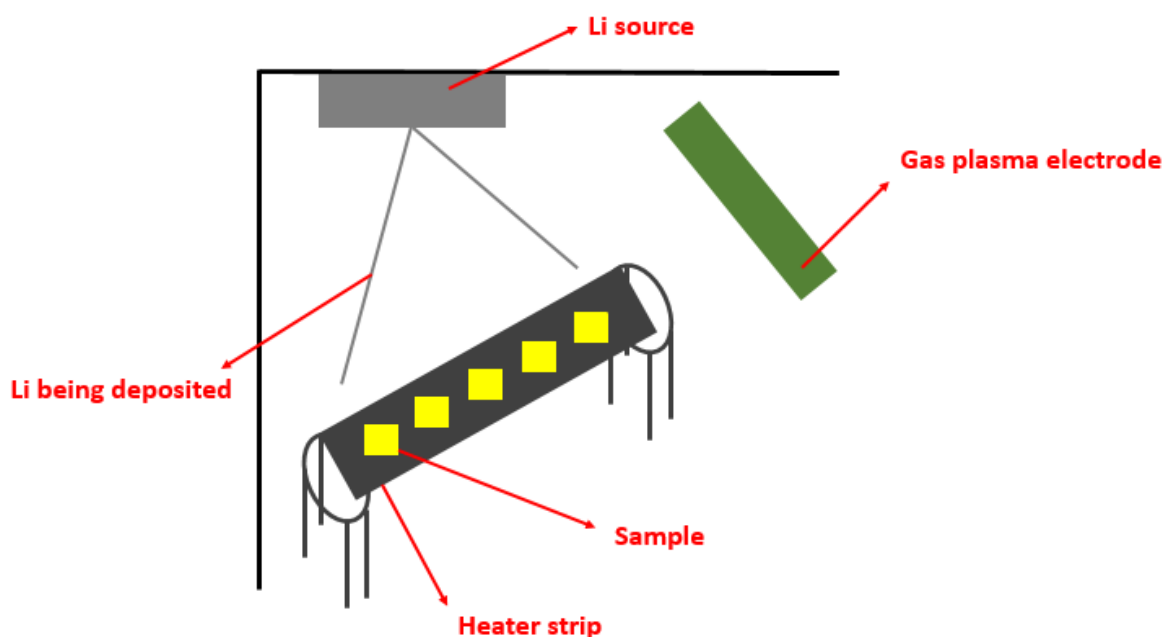


Figure 4.0: A schematic diagram of the Balzer 510 coating machine.

4.1.1 Batch 1

Batch 1 was assembled with the aim of assessing the different oxidation times of the substrates, deducing the optimum. Additionally, an evaluation of the efficacy of the polymer, carboxyethyl silanetriol sodium salt (25 wt% in water) was made.

Step 1: 4 × BeCu, 2 × Ag and 2 × Ni samples were cleaned, as explained in section 4.1.0.1.

Step 2: The BeCu samples were oxidised for 1 minute (BeCu(1 min)), 5 minutes (BeCu(5 min)) and 30 minutes (BeCu(30 min)), one BeCu sample was left un-oxidised. One of each Ag and Ni samples were oxidised for 30 minutes, (Ag(30 min)) and (Ni(30 min)), respectively. Again, the remaining Ag and Ni samples were left un-oxidised.

Step 3: Each sample was seeded with the polymer, carboxyethyl silanetriol sodium salt (25 wt% in water) via a drop cast method. The polymer was left on each sample for 15 minutes. The samples were then washed in deionized water for approximately 3 seconds and then dried with an air gun. The next stage was similar to the previous, however, involved seeding the sonicated diamond as opposed to the polymer. A self-assembly on each sample was now achieved, as discussed in section 4.1.0.3.

Step 4: All the samples were annealed, O-terminated and then lithiated, as described in section 4.1.0.4.

4.1.2 Batch 2

The objective behind Batch 2 was to, once again, analyse the different oxidation times of the substrates, but this time, with an alternative polymer, poly(ethyleneimine) (5 wt% in water). A comparison could be made between the two polymers used in batches 1 and 2, deducing which one is more effective. Finally, an evaluation of the two seeding methods, the drop cast method and the submerging method, was made.

Step 1: 5 × BeCu, 2 × Ag and 2 × Ni samples were cleaned, as explained in section 4.1.0.1.

Step 2: The BeCu samples were oxidised for 1 minute (BeCu(1 min)), 5 minutes (BeCu(5 min)), two samples were oxidised for 30 minutes (BeCu(30 min)) and one BeCu sample was left un-oxidised. One of each Ag and Ni samples were oxidised for 30 minutes, (Ag(30 min)) and (Ni(30 min)), respectively. Again, the remaining Ag and Ni samples were left un-oxidised. The oxidation levels were varied for the same reason as Step 2 for batch 1.

Step 3: All the samples, with the exception of one of the BeCu(30 min) samples, were seeded with a different polymer, poly(ethyleneimine) (5 wt% in water) via a drop cast method. The polymer was left on each sample for 15 minutes. The remaining BeCu(30 min) sample was submerged into the polymer solution for 15 minutes, as opposed to drop casted. All the samples were then washed in deionized water for approximately 3 seconds and then dried with an air gun. The sonicated diamond was then seeded on top of the polymer using a drop cast method, forming a self-assembly, described in section 4.1.0.3.

Step 4: All the samples were annealed, O-terminated and then lithiated, as described in section 4.1.0.4.

4.1.3 Batch 3

Batch 3 was designed with the intension of determining which concentration of the polymer, poly(ethyleneimine), is the more effective, using BeCu (30min) as the substrate and a submersion method for seeding a polymer.

Step 1: 4 × BeCu were cleaned, as explained in section 4.1.0.1.

Step 2: The BeCu samples were all oxidised for 30 minutes (BeCu(30 min)).

Step 3: Each sample was seeded with, poly(ethyleneimine) at different concentrations in water: 5, 1, 0.5, 0.1 wt%, by submerging all 4 samples for 15 minutes. They were then washed in deionized water for approximately 3 seconds and then dried with an air gun. Similar to batches 1 and 2, the diamond was seeded via a drop cast method and achieved a self-assembly, discussed in section 4.1.0.3. This step achieved a self-assembly on each sample, as discussed in section 4.1.0.3.

Step 4: All the samples were annealed, O-terminated and then lithiated, as described in section 4.1.0.4.

4.2 Sample Characterisation Method

4.2.0 Raman Spectroscopy

In Raman spectroscopy, a sample is irradiated with a high frequency monochromatic light source^[127] and the scattered radiation is detected. Two mechanisms occur before detection^[128]. In the first, the sample makes an upward transition between two molecular energy levels, E_1 and E_2 , whereas, in the second, the sample makes a downward transition resulting in emissions at frequencies $h\nu_M = E_1 - E_2$ and $h\nu_M = E_1 + E_2$, respectively^[128]. The former, called the Stokes Raman transition, causes radiation of lower frequencies and is the radiation that is detected. The latter, called the anti-Stokes Raman transition, causes radiation of a higher frequency. These can be seen in figure 4.1.

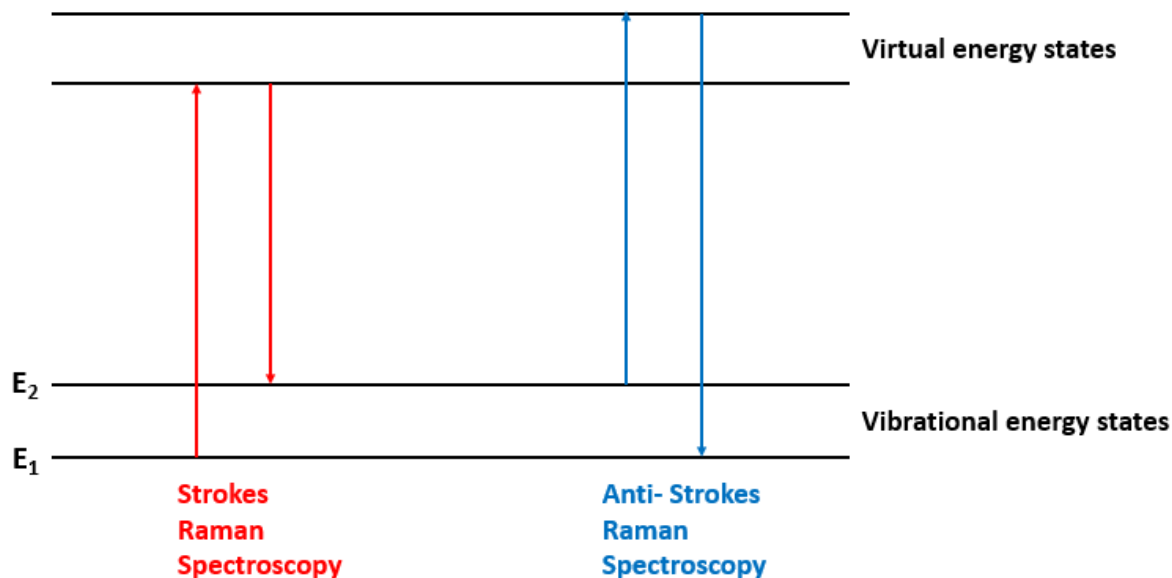


Figure 4.1: Vibrational Raman Scattering, showing the absorption of radiation between actual and virtual vibrational states, inspired from^[129].

Method: Raman Spectroscopy (Model: Renishaw 2000), situated in the School of Chemistry, University of Bristol, was executed using a 532 nm, Green, Ar⁺ laser. Two samples were measured: the diamond suspension and the BeCu (30 min), PEI 0.5 wt%, Li-O-terminated diamond self-assembly.

4.2.1 Scanning Electron Microscopy

Scanning electron microscopy (SEM) is an important tool for studying the morphology on the surface of a sample. A very fine ‘probe’ of electrons are accelerated from a thermionic or field emission source with typical energies between 1 keV and 30 keV^[130]. This electron beam is focused at the surface of the sample and scans across the sample in a ‘raster’ or pattern of parallel lines^[131].

When the incident electron enters the sample, the electrons in the sample are ejected out of their orbital shells, thus ionizing the atom. The secondary electrons which escape from the surface have kinetic energies of ~ 50 eV^[130]. If these secondary electrons are within 10 nm^[131] of the sample surface, they are detected.

A backscattered electron arises when the incident electron collides with the nucleus of a sample of a surface atom and is reflected backwards from the surface. Unlike secondary electrons, these electrons have energies between 50 eV and that of the incident electron^[130].

Method: SEM was measured using a field emission gun (JEOL IT300) at the School of Chemistry, University of Bristol. The diamond samples produced in batches 1, 2 and 3 were assessed. The fractional coverage and surface morphology of each sample was analysed.

4.2.2 Contact Angle

The contact angle, θ , is derived from Young’s equation^[132], equation 4.0, where γ_L , γ_S and γ_{SL} are the surface tension of the liquid, solid and solid-liquid interface, respectively.

$$\gamma_L \cos\theta = \gamma_S - \gamma_{SL} \quad \text{eq. 4.0}$$

This equation gives a quantitative description of the wetting phenomena. If a liquid is placed on a solid surface, the liquid can either: wet completely ($\theta = 0^\circ$) or form a finite contact angle^[131] ($\theta > 0^\circ$). In the latter case, a wetting line is established between the three-phases: the solid, the liquid and the vapour, depicted in figure 4.2. Here, the contact angle is $< 90^\circ$, this corresponds to a hydrophilic, polar surface, where adhesive forces between the solid and the liquid promote wetting. Conversely, if the contact angle is $> 90^\circ$, this corresponds to the cohesive forces which minimise wetting.

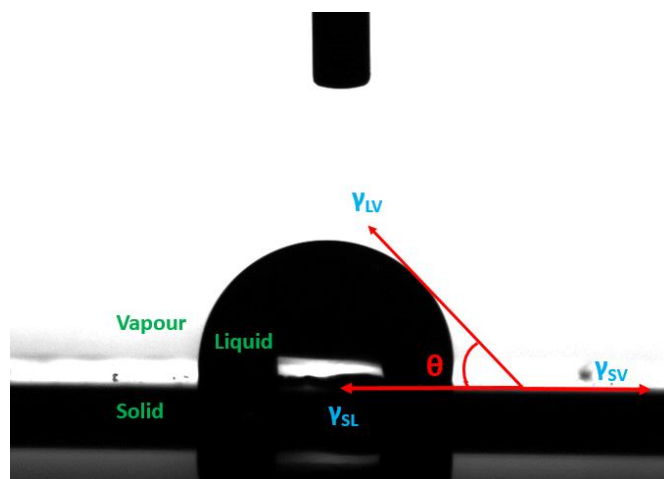


Figure 4.2: A droplet of deionized water on the surface of the BeCu(5 min) sample, showing the contact angle, θ . In this example, θ is $< 90^\circ$ which corresponds to a hydrophilic surface. This figure also illustrates the surface tension of the solid-liquid, liquid-vapour and solid-vapour interfaces, labelled γ_{SL} , γ_{LV} and γ_{SV} , respectively.

Method: Contact angle measurements were made using the KRÜSS Drop Shape Analyzer, DSA100 in the KRÜSS Centre in the School of Chemistry, University of Bristol. 3 μL of deionised water was dropped onto the samples using a micro syringe, with a diameter of 0.515 mm, under standard conditions. Depending on the angle, the programme used either the tangent-1 or the circle methods to calculate the contact angle. The former was used for larger contact angles and the latter for the smaller contact angles. Both calculations assumed an elliptical drop. Video recordings at 25 frames per second were taken for each sample. The final contact angle was deduced from when the contact angle measurements plateaued.

4.2.3 Secondary Electron Emission Yield

The theory behind secondary electron emission involves the detection of secondary electrons upon bombardment of primary electrons, discussed in section 2.8. The equipment used was the JEOL JSM-6100 Scanning Microscope at the Department of Physics, University of Bristol, and the experiment proceeded under vacuum levels of 10^{-10} Torr. This SEM setup employed a tungsten thermionic emission gun with a current between 4×10^{-12} and 1×10^{-11} and an energy ranging between 0.6 and 10 keV. The penetration depth of these primary electrons was 120 nm at 1200 eV. A magnetic lens was necessary to focus the electron beam to a desired spot size. A Farady Cup, comprised of

machined aluminium, was positioned inside the chamber and collected the secondary electrons emitted.

Unfortunately, due to a fault, the JOEL JSM-6100 Scanning Microscope was out of commission for batches 2 and 3 of this experiment. Instead, a prediction of the results will be made.

5 Results and Discussion

5.0 Preliminary Tests

5.0.0 Raman Spectroscopy

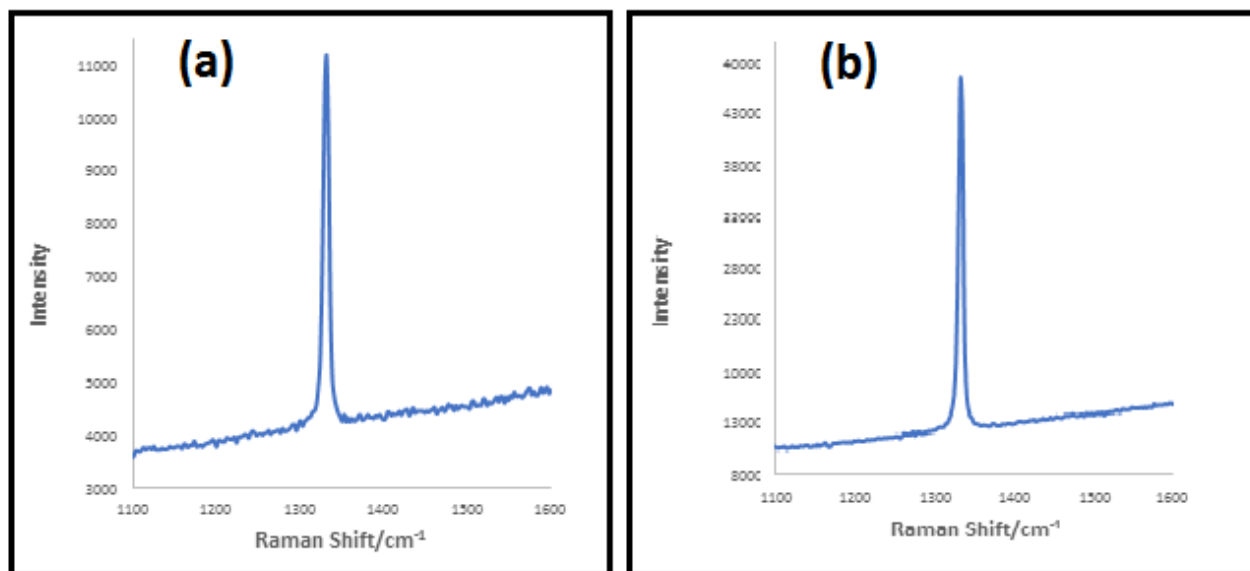


Figure 5.0: Raman Spectroscopy of (a) the diamond suspension and (b) the BeCu(30 min) sample, seeded with PEI and diamond, annealed and OLi-terminated.

The spectra in figure 5.0 confirms the presence of sp³ diamond in, (a) the suspension and (b) self-assembled diamond sample, at the characteristic peak of 1322 cm⁻¹, with no evidence of graphite, detected at 1585 cm⁻¹^[133].

5.0.1 Contact Angle Measurements

| Name of Sample | Contact angle $\theta(L)$ / ° | Contact angle $\theta(R)$ / ° |
|----------------|-------------------------------|-------------------------------|
| BeCu | 85.9 | 85.6 |
| BeCu (1 min) | 66.2 | 69.5 |
| BeCu (5 min) | 55.1 | 54.9 |
| BeCu (30 min) | 49.9 | 48.7 |
| Ag | 24.5 | 24.5 |
| Ag (30 min) | 93.1 | 96.7 |
| Ni | 88.8 | 89.4 |
| Ni (30 min) | 11.6 | 11.6 |
| Single Crystal | 77.2 | 77.0 |

Figure 5.1: Contact angles, θ , for the left (L) and the right (R) side of the deionized water droplet on the cleaned samples, oxidised for various times.

Contact angle measurements for the BeCu samples revealed an overall decrease in the size of the angle as the oxidation times were increased. A similar trend was true for the Ni samples. This suggests that, as the oxidation of each sample was increased, the surfaces became more polar/hydrophilic due to the adhesive forces promoting wetting, explained in section 4.2.2.

The opposite trend was observed for the Ag samples. The Ag(30 min) sample minimised the wetting, thus increasing the contact angle. After oxidation for 30 minutes, the Ag sample formed a thin black layer on the surface, characteristic of Ag_2O , which is a hydrophobic oxide of Ag.

The single crystal was included for comparison reasons, however, due to the lack of resources, the single crystal will not appear in further results.

For the majority of the results, there was a variation between the left and right side of the droplet. This was due to the uneven surface of the substrates.

5.0.2 Zeta potential

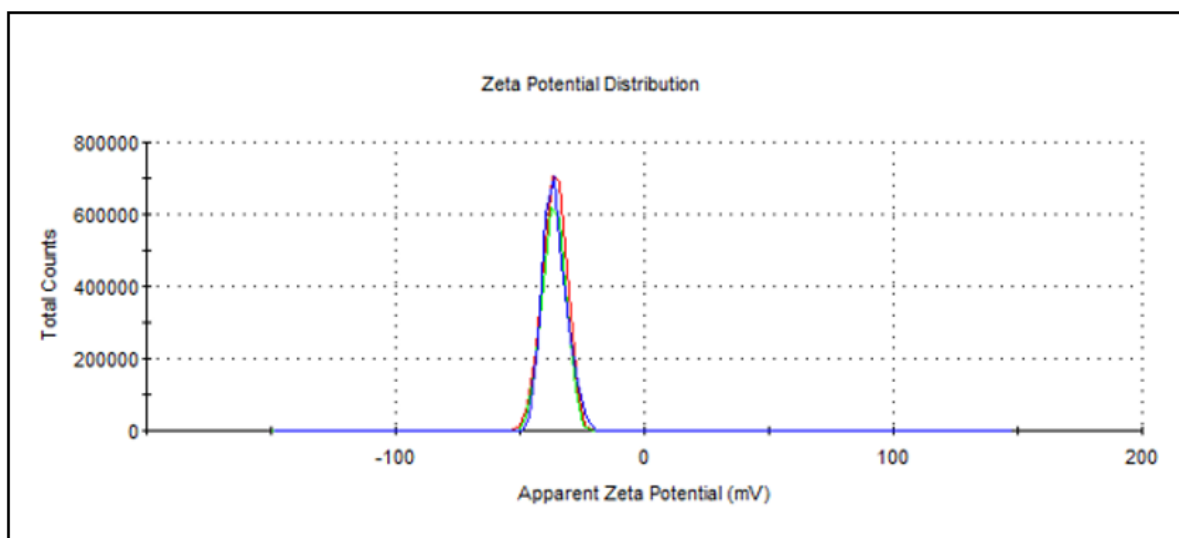


Figure 5.2: Zeta potential of the diamond suspension, sonicated for 4 hours, at -35.0 mV.

The negative potential of the diamond suspension displayed in figure 5.2 confirmed the requirement of a positive layer between the substrates and the diamond, in the form of a cationic polymer, the structures of which can be found in section 3.

5.0.3 Scanning Electron Microscopy

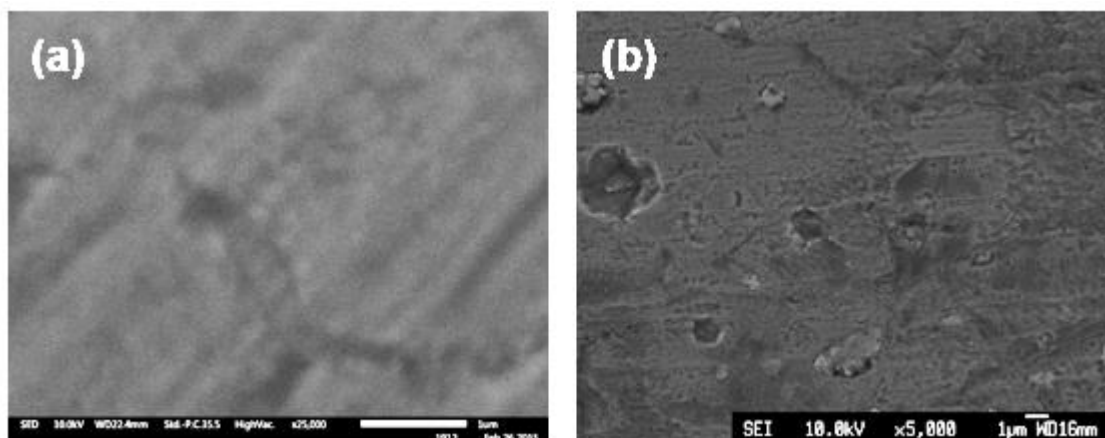


Figure 5.3: SEM images of (a) BeCu seeded with carboxyethyl silanetriol sodium salt (25 wt% in water) and (b) BeCu seeded with poly(ethyleneimine) (5 wt% in water).

This test was carried out to inspect the surface of the polymers. This subsequently ensured that a differentiation could be established in upcoming tests between the diamond and the polymer. These images reflect no contribution to the structural morphology and texture of the surface.

5.1 Batch 1

5.1.0 Contact Angle measurements

| Name of Sample | Contact angle $\theta(L)$ / ° | Contact angle $\theta(R)$ / ° |
|----------------|-------------------------------|-------------------------------|
| BeCu | 18.9 | 18.9 |
| BeCu (1 min) | 18.2 | 18.2 |
| BeCu (5 min) | 17.0 | 17.0 |
| BeCu (30 min) | 12.2 | 12.2 |
| Ag | 10.1 | 10.1 |
| Ag (30 min) | 15.8 | 15.8 |
| Ni | 22.8 | 22.8 |
| Ni (30 min) | 9.3 | 9.3 |

Figure 5.4: Contact angles, θ , for the left (L) and the right (R) side of the deionized water droplet on the various substrates which have been seeded with carboxyethyl silanetriol sodium salt (25 wt% in water) and diamond. The samples all annealed, O-terminated and lithated.

All the samples in figure 5.4 were seeded with carboxyethyl silanetriol sodium salt (25 wt% in water) and diamond, forming self-assembled layers, and were functionalised with a LiO-terminated surface. Overall, the contact angles have decreased in comparison to the samples tested prior to self-assembly, in section 5.1.1. Despite the general decrease, the same trends are seen; as the oxidation of the BeCu and Ni increase, the contact angles decrease. This suggests that as the oxidation increases, there was a stronger interaction with the cationic polymer, and a better coverage was achieved. This in turn meant that more diamond was assembled onto the polymer, so more could be LiO-terminated. As mentioned in section 4.1.0.6, a LiO-terminated surface is very hydrophilic and polar, promoting an increase in wetting.

Again, a similar trend was seen in the Ag samples as was seen in section 5.1.1. As the oxidation increased, the contact angle also increased. The hydrophobic nature of Ag_2O meant that the Ag(30 min) sample had a poor polymer coverage and less diamond was seeded. Hence, a less concentrated LiO-terminated surface, thus wetting was aided.

5.1.1 Scanning Electron Microscopy

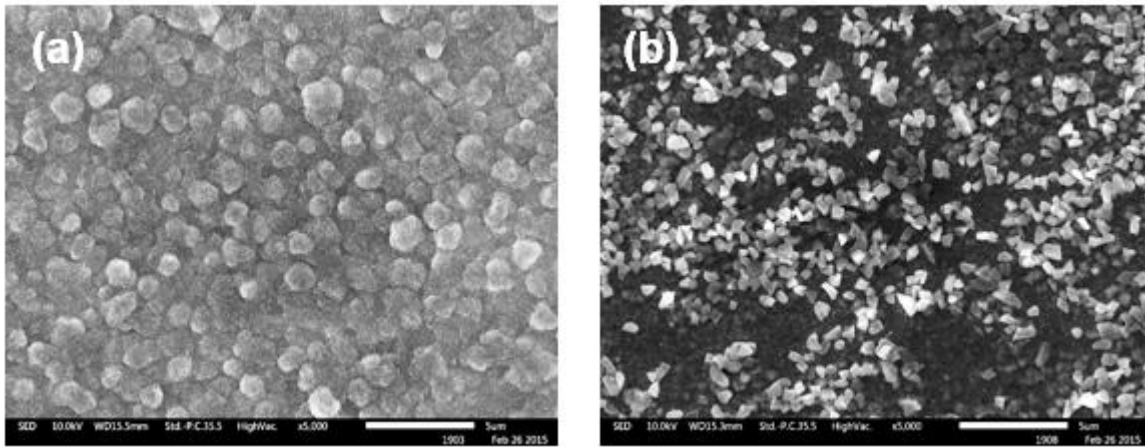


Figure 5.5: SEM images of (a) Ag and (b) Ni. Both samples were seeded with carboxyethyl silanetriol sodium salt (25 wt% in water) and diamond. The samples were then all annealed, O-terminated and lithated.

The SEM images in figure 5.5 demonstrate two very different morphologies of diamond, as a result of the heat treatment they received. Annealing is capable of altering the physical and chemical properties of a material, which was discussed in section 4.1.0.5.

The Ag sample is presented in figure 5.5(a). Ag has a tendency to move around during the annealing process. In doing so, a presumption can be made that the sample had agglomerated. The sample had 100 % fractional coverage. It is important to note that for every sample produced in this thesis, there were localised areas of higher diamond density.

The Ni sample is displayed in figure 5.5(b), with diamond particle sizes between 0.5 and 1 μm . The fractional coverage was $\sim 70\%$.

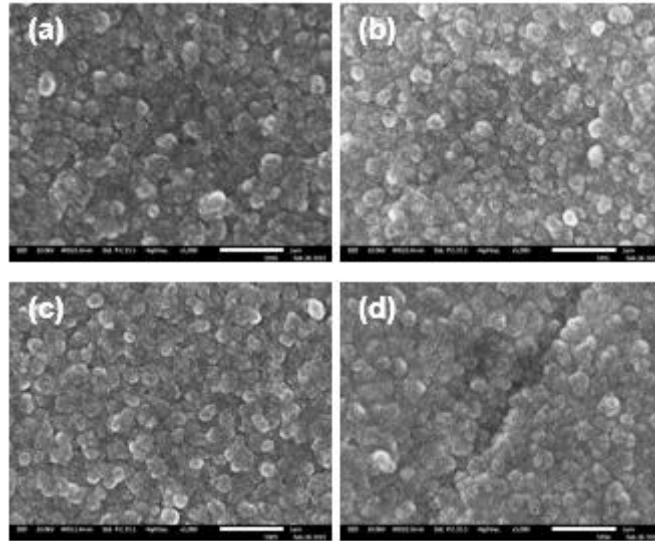


Figure 5.6: SEM images of (a) BeCu, (b) BeCu(1 min), (c) BeCu(5 min) and (d) BeCu(30 min). All samples were seeded with carboxyethyl silanetriol sodium salt (25 wt% in water) and diamond. The samples were then all annealed, O-terminated and lithated.

Evaluation of the four SEM images for each oxidation demonstrated a good coverage, as well as a consistent morphology. The size of the diamond particles was between 2 and 3 μm . The fractional coverage for all the samples was 100 %, so a high SEEY would be expected for all samples.

5.1.2 Luminescence

During the low pressure glow discharge plasma treatment of these samples, the diamond layers emitted green-yellow luminescence due to the VUV exciting the nitrogen colour centres in the diamond particles. The BeCu samples gave the brightest and most even light. Whereas the Ag and Ni presented the same luminescence, the light was considerably dimmer. Again, this result suggests a high SEEY is anticipated for the BeCu samples.

5.1.3 Secondary Electron Emission Yield

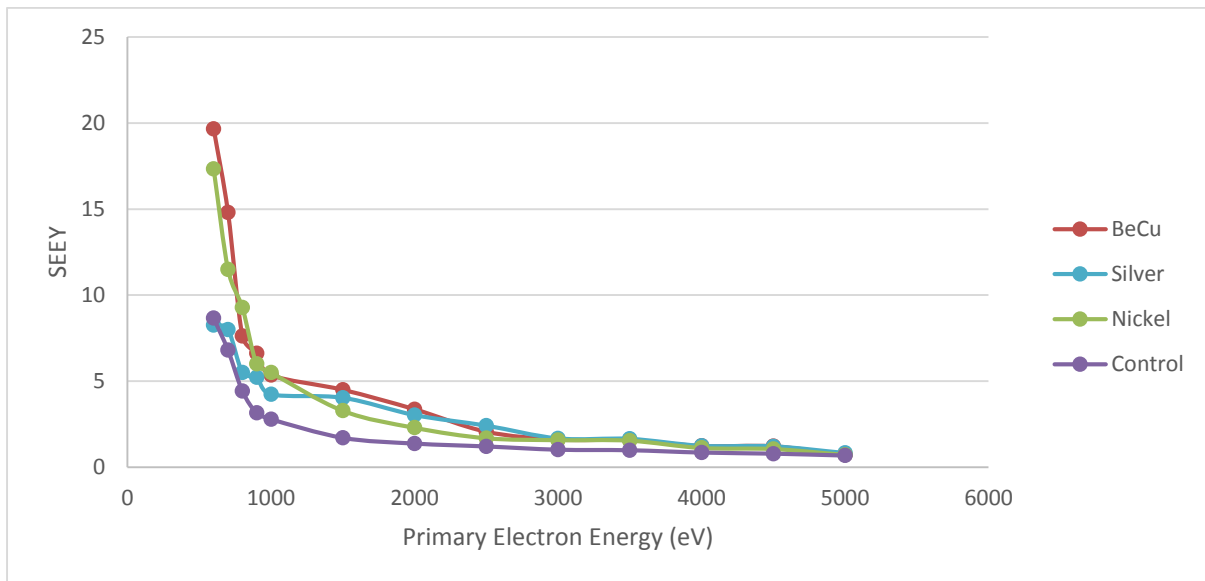


Figure 5.7: SEFY for BeCu(30 min) in red, Ag(30 min) in blue, Ni(30 min) in grey and BeCu in yellow. The yields at 600 eV were, 19.7, 8.25, 17.33 and 8.67, respectively. The first three samples were from batch 1, the last sample, BeCu, was just the metal substrate and acted as a control for the experiment.

From figure 5.7, a deduction can be made that the highest yielding self-assembly was the BeCu(30 min) sample. The sample which yielded the lowest secondary electrons was the Ag(30 min) sample. All the samples had a higher yield than the BeCu control, confirming diamond's ability to yield the highest numbers of secondary electrons.

5.2 Batch 2

5.2.0 Contact Angle Measurements

| Name of Sample | Contact angle $\theta(L)$ / ° | Contact angle $\theta(R)$ / ° |
|----------------|-------------------------------|-------------------------------|
| BeCu | 18.3 | 18.3 |
| BeCu (1 min) | 15.9 | 15.9 |
| BeCu (5 min) | 13.5 | 13.5 |
| BeCu (30 min) | 12.0 | 12.0 |
| Ag | 13.2 | 13.2 |
| Ag (30 min) | 29.9 | 29.9 |
| Ni | 13.9 | 13.9 |
| Ni (30 min) | 7.7 | 7.7 |

Figure 5.8: Contact angles, θ , for the left (L) and the right (R) side of the deionized water droplet on the various substrates which have been seeded with poly(ethyleneimine) (5 wt% in water) and diamond. The samples were all annealed, O-terminated and lithiated.

The contact angle measurements had the same trend as seen in section 5.2.0 from batch 1. For the same reasons, the contact angles of the BeCu and the Ni samples decreased with increasing oxidation, whereas the opposite trend was true for the Ag samples.

5.2.1 Scanning Electron Microscopy

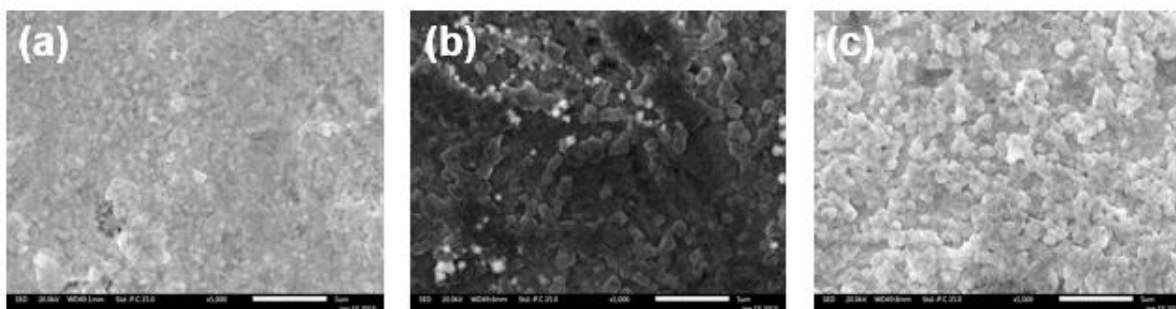


Figure 5.9: SEM images of (a) Ag(30 min), (b) Ni(30 min) and (c) BeCu(30 min). All samples were seeded with Poly(ethyleneimine) (5 wt% in water) and diamond. All the samples contain an OLi-terminated surface.

The images in figure 5.9 revealed that the Ag(30 min) sample had the least amount of diamond deposited. The Ni(30 min) sample possessed more diamond on the surface, however, there were localised areas of higher diamond density, and regions where the diamond was not evenly distributed. This indicated a lower surface area of diamond, which would result in a lower secondary emission. The BeCu(30 min) sample, however, showed a more disperse diamond distribution, with a better coverage. This suggested a higher secondary electron emission would be expected from this sample.

5.2.2 Luminescence

The same result for luminescence seen for batch 1 occurred, however, the submerged BeCu(30 min) sample emitted the brightest light, for similar reasons explained in section 5.2.2.

5.2.3 Secondary Electron Emission Yield

After analysis of the above results, and from observation of the samples, I would predict that the BeCu samples would yield the highest secondary electron emission. The SEM images confirm that there is more diamond present on the surface of these samples in comparison to the Ag and Ni samples. Furthermore, during the functionalization of the samples, the BeCu samples emitted the brightest light, again, demonstrating that there was more diamond on the surface of these samples. From the contact angle results, a conclusion can be made that the BeCu samples were more hydrophilic as the oxidation increased, which could result in a stronger interaction with the cationic polymer. Hence, a prediction could be made that the BeCu(30 min) sample would yield the highest secondary electrons. From observing the samples, the BeCu(30 min) sample which had been submerged in the polymer solution for 15 minutes revealed the best, most even coverage of diamond. This was confirmed in the functionalization treatment, as this gave the brightest luminescence. This is, of course, a prediction, and the result will remain inconclusive until the quantitative SEEY is obtained.

5.3 Batch 3

5.3.0 Contact Angle Measurements

| Name of Sample | Contact angle $\theta(L)$ /° | Contact angle $\theta(R)$ /° |
|---------------------------|------------------------------|------------------------------|
| BeCu (30min), PEI 5 wt% | 12.0 | 12.0 |
| BeCu (30min), PEI 1 wt% | 11.8 | 11.8 |
| BeCu (30min), PEI 0.5 wt% | 11.3 | 11.3 |
| BeCu (30min), PEI 0.1 wt% | 10.7 | 10.7 |

Figure 5.10: Contact angles, θ , for the left (L) and the right (R) side of the deionized water droplet on BeCu(30 min). Each sample was seeded with different poly(ethyleneimine) concentrations of 5, 1, 0.5 and 0.1 wt%. The samples were all annealed, O-terminated and lithated.

The hydrophobicity on the surface of the samples increased with decreasing polymer concentration. The polymer with the 0.1 wt% had the more polar surface, thus was the optimum polymer concentration for this experiment.

5.3.1 Scanning Electron Microscopy

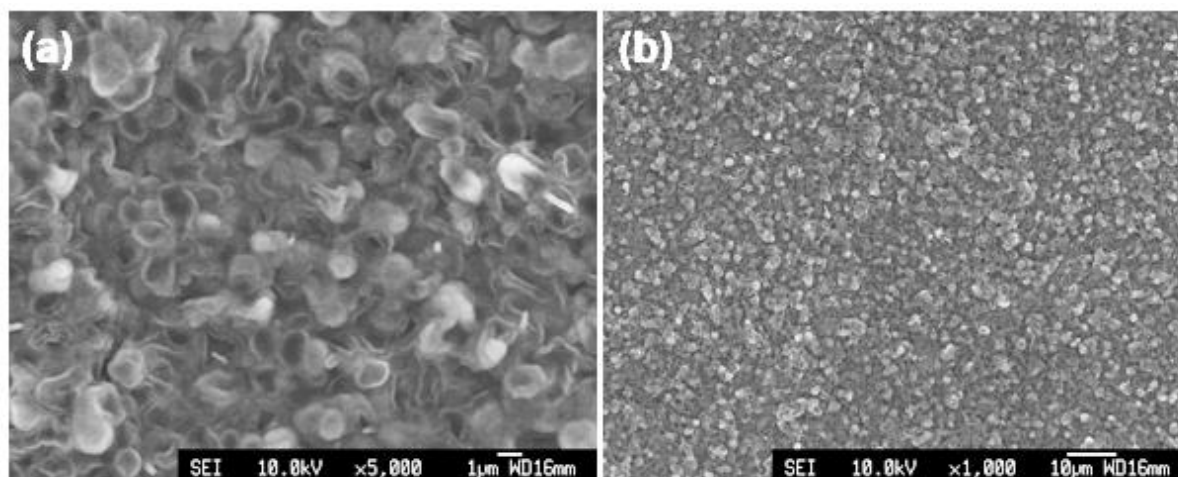


Figure 5.11: SEM images of BeCu(30 min) seeded with poly(ethyleneimine) (0.1 wt% in water) and diamond. This sample was annealed, O-terminated and lithiated, at two different magnifications.

The images in figure 5.11 display the surface of the 0.1 wt% polymer sample. This one was chosen to be displayed on account of the contact angle result in section 5.4.0. The coverage of diamond on the surface is even and the particle sizes are uniform.

5.3.2 Luminescence

Similarly, the same result for luminescence seen for batches 1 and 2 occurred and for the same reasons. The sample which emitted the most light was the BeCu 0.1 wt% sample.

5.3.3 Secondary Electron Emission Yield

A prediction for the SEE yields of these samples can be made. The BeCu(30 min) sample with 0.1 wt% of PEI demonstrated the lowest contact angle of all the samples. The image of this sample also displayed a very even, homogenous layer of diamond on the surface. Furthermore, research has been done^[27] that looked at the different concentrations of the PEI polymer on diamond self-assemblies. Although the polymer used for this study was slightly different to the one used in this thesis, the conclusion was made that the PEI polymer at 0.1 wt% gave the optimum diamond coverage on the surface.

6 Conclusion

A conclusive result can be made for batch 1. This batch used carboxyethyl silanetriol sodium salt (25 wt% in water) as the polymer. The BeCu(30 min) sample had a contact angle measurement of 12.2/12.2 on the left and right side of the droplet. The SEM image for this sample revealed the more even and fully coated diamond surface. It also emitted the brightest luminescence during the functionalization procedure. It was, therefore, no surprised that this sample yielded the highest secondary electron emission, 19.7 at 600 eV. Therefore, BeCu was the favoured metal substrate, and the optimum oxidation time for BeCu was 30 minutes.

The other two batches remain inconclusive. A comparison of the contact angle measurements can be made, however, between the BeCu(30 min) from the preliminary tests, the BeCu(30 min) sample from batch 1 and the BeCu(30 min) sample from batch 2, which used poly(ethyleneimine) (5 wt% in water) as the polymer, as well as the other oxidation times, and can be seen in figure 6.0. The latter produced a contact angle measurement of 12.0/12.0 of the left and right side of the droplet. A 0.2 degree decrease from the BeCu(30 min) sample from batch 1 and a 37.9/36.7 degree decrease from the BeCu(30 min) sample from the preliminary test. This indicated an increase in hydrophilicity of the surface, which would imply a great OLi-terminated surface was present.

BeCu Samples

| Oxidation times (minutes) | Preliminary Test | Batch 1 | Batch 2 |
|---------------------------|------------------|-----------|-----------|
| 0 | 85.9/85.6 | 18.9/18.9 | 18.3/18.3 |
| 1 | 66.2/69.5 | 18.2/18.2 | 15.9/15.9 |
| 5 | 55.1/54.9 | 17.0/17.0 | 13.5/13.5 |
| 30 | 49.9/48.7 | 12.2/12.2 | 12.0/12.0 |

Figure 6.0: A compilation of the results using BeCu as the substrate. The preliminary tests use just BeCu with no self-assembly, as discussed in section 4.0. Batch 1 is a diamond self-assembly with carboxyethyl silanetriol sodium salt as the polymer. Batch 3 is also a diamond self-assembly, but uses poly(ethyleneimine) 5 wt% as the polymer.

Correspondingly, a comparison can be made between the Ag and Ni batches, demonstrated in figures 6.1 and 6.2. The contact angle measurements of the Ag samples are at their lowest with the carboxyethyl silanetriol sodium salt polymer from batch 1. The contact angles increase in batch 2 as the polymer changes to poly(ethyleneimine). The largest contact angle measurements are displayed in the preliminary test, verifying that the oxide of Ag, Ag₂O has a hydrophobic surface, and that the Ag surface is less hydrophilic that with the diamond self-assembly. The Ni trends are similar to BeCu trends. The contact angles decrease from bare Ni and Ni(30 min) from the preliminary tests, to the Ni and Ni(30 min) samples from batch 2.

Ag Samples

| Oxidation times (minutes) | Preliminary Test | Batch 1 | Batch 2 |
|------------------------------|------------------|-----------|-----------|
| 0 | 24.5/24.5 | 10.1/10.1 | 13.2/13.2 |
| 30 | 93.1/96.7 | 15.8/15.8 | 29.9/29.9 |

Figure 6.1: A compendium of the results using Ag as the substrate. The preliminary tests use just Ag with no self-assembly, as discussed in section 5.1.1. Batch 1 is a diamond self-assembly with carboxyethyl silanetriol sodium salt as the polymer. Batch 3 is also a diamond self-assembly, but uses Poly(ethyleneimine) 5 wt% as the polymer.

Ni Samples

| Oxidation times (minutes) | Preliminary Test | Batch 1 | Batch 2 |
|------------------------------|------------------|-----------|-----------|
| 0 | 88.8/89.4 | 22.8/22.8 | 13.9/13.9 |
| 30 | 11.6/11.6 | 9.3/9.3 | 7.7/7.7 |

Figure 6.2: a compilation of the results using Ni as the substrate. The preliminary tests use just Ni with no self-assembly, as discussed in section 4.0. Batch 1 is a diamond self-assembly with carboxyethyl silanetriol sodium salt as the polymer. Batch 3 is also a diamond self-assembly, but uses Poly(ethyleneimine) 5 wt% as the polymer.

Likewise, a comparison can be made between the BeCu(30 min) sample from batches 1 and 2 (using carboxy silanetriol sodium salt and polyethyleneimine (5 wt%), respectively) with the BeCu(30 min) sample from batch 3 using the lowest concentration of poly(ethyleneimine) (0.1 wt% in water), this is summarised in figure 6.3. The contact angle measurements decreased from 12.2/12.2 to 12.0/12.0 to 10.7/10.7 on the left and right hand side of the droplet. This is a decrease of 1.5 and 1.3. Thus, the latter has a more polar surface and would be expected to have a higher secondary electron emission yield. So, the predicted trend would be, as the oxidation of the substrate increases and as the concentration of the poly(ethyleneimine) decreases, the SEEY increases.

BeCu(30 min) Samples

| Batch 1 (carboxyethyl silanetriol sodium salt) | Batch 2 (Poly(ethyleneimine) 5 wt%) | Batch 3 (Poly(ethyleneimine) 0.1 wt%) |
|---|--|--|
| 12.2/12.2 | 12.0/12.0 | 10.7/10.7 |

Figure 6.3: A compilation of the results using BeCu(30 min) as the substrate. Batch 1 had the largest contact angles. As the concentration of the polymer, poly(ethyleneimine) decreased, the contact angle correspondingly decreased.

A comparison between the SEM images of the three samples just mentioned can be made. The uniformity and coverage improved from batches 1 to 3, with a larger surface area of diamond observed for the BeCu(30 min) with the 0.1 wt% of poly(ethyleneimine), which would suggest a higher secondary electron emission yield.

Finally, in batch 2, an experiment was done to study the seeding methods. Two BeCu(30 min) samples were seeded with poly(ethyleneimine) (5 wt% in water), via a drop cast method and via submersion. Inspection of the samples concluded that a more even layer of diamond could be seen on the surface of the latter sample. The nature of drop casting means a dome-like shape is formed on the surface of the substrate which does not cover the edges properly. Submerging the substrate in the polymer, however gives an even, flat layer of the polymer on the surface.

7 Further Work

Most importantly, completing this work by evaluating the secondary electron emission yield of batches 2 and 3 is vital in completing the story and concluding which polymer and of which polymer concentration gives the optimum result.

One problem encountered in these experiments was the drying of the samples with the air gun post seeding. With this method, the nature of drying results in the polymer and diamond getting blown to one side of the sample, creating a ripple effect on the surface. The aim of this project was to optimise the SEEY, so an even distribution of diamond across the surface was favourable. Devising another method of drying is important.

Another polymer, such as polyallyldimethylammonium chloride (PDDA) may be used to evaluate its ability to act as a 'glue' between the substrate and the diamond, and comparing these results with the carboxyethyl silanetriol sodium salt and the poly(ethyleneimine) samples.

Taking SEM images of the samples before the heat treatment and surface termination to study the morphology of the diamond prior to functionalization. This would give an indication as to whether this functionalization has an effect on the size and shape of the diamond, but could also reveal the contribution of the metal to the morphology of the diamond.

The BeCu oxidised for 30 minutes yielded the highest SEEY from batch 1. This was the longest oxidation time observed, so a further experiment can be done to look at longer oxidation times which could produce a more optimum self-assembly.

8 References

- [1] P. W. May, *Phil. Trans. R. Soc. Lond. A*, 2000, 358, 473-495
- [2] J. Y. Dickerson, *The Book of Diamond's Dover Publishers*, New York, 1965, 2, 3-5
- [3] P. W. May, *CVD Diamond – a new technology for the future?*, Endeavour magazine, 1995, 19, 101-106
- [4] P. W. May, *Science*, 2008, 319, 1490-1491
- [5] M. H. Nazaré and A. J. Neves, *Properites, Growth and Applications of Diamond*, INSPEC, London, 2001
- [6] J. Wilks, E. Wilks, *Properties and Applications of Diamond*, Butterworth Heinemann, 1991, 1, 1-3
- [7] T. R. Marshall, R. Baxter-Brown, *Journal of Geochemical Exploration*, 1995, 53, 277-292
- [8] F. P. Bund, *J. Geo Research*, 1980, 85, 6930-6936
- [9] K. E. Spear, J. P. Dishumes, *Synthetic Diamond: Engeneering CVD Science and Technologies*, John Wiley & Sons, New York, 1994, 1, 47
- [10] Y. Lifshitz, T. Köhler, T. Frauenheim, I. Guzman, A. Hoffman, R. Q. Zhang, X. T. Zhou, S. T. Lee, *Science*, 2002, 297, 1531-1533
- [11] C. H. Desch, *The Chemistry of Solids*, Cornell University Press, Ithaca, NY, 1934, 180
- [12] A. K. Geim, K. S. Novoselov, *Nature Materials*, 2007, 6, 183-191
- [13] A. K. Geim, *Science*, 2009, 342, 1530, 1534
- [14] T. E Brown, H. E. LeMay, B. E. Bursten, *Chemistry The Central Science*, Uppersaddle River, NJ: Simon & Schuster, 1997, 412-413
- [15] A. Shih, J. Yater, P. Pehrsson, J. Butler, C. Hor and R. Abrams, *J. Appl. Phys.*, 1997, 82, 1860-1867
- [16] O. Hachenberg and W. Bbrauer, *Advances in Electronics and Electron Physics*, Academic Press, New York, 1959, 1, 413
- [17] F. Maier, M. Riedel, B. Mantel, J. Ristein, and L. Ley, *J. Phys. Rev. Lett.*, 2000, 85, 3472-3475
- [18] L. S. Pan, *Diamond: Electronic Properties and Applications*, Kluwer Academic Publishers, USA, 1995, 1, 320
- [19] C. Cytermann, R. Brener and R. Kalish, *Diam. Relat. Mater.*, 1994, 3, 677
- [20] G. G. Fountain, R. A. Rudder, D. P. Matta, S. V. Hattangady, R. G. Alley, G. C. Hudson, J. B. Potshill, R. J. Markunas, T. P. Humphreys, R. J. Nemanich, V. Venkatesan and K. Das, *Diamond Materials, Proc. 2nd Symp. Electrochem. Soc.*, 1991, 523
- [21] G. Popovici, T. Sung, S. Khasawinah, M. A. Prelas, *J. Appl. Phys.*, 1995, 77, 5625
- [22] V. S. Vavilov, M. I. Guseva, E. A. Konorova, V. V. Krasnopevtsev, V. F. Sergienko and V. V. Tutov, *Soviet Physics – Solid State*, 1966, 8, 1560-1561
- [23] N. Fujimori, T. Imai and A. Dori, *Vacuum*, 1986, 36, 99-102
- [24] R. Haubner and D. Sommer, *Diam. Relat. Mater.*, 2003, 12, 298-305
- [25] E. B. Lombardi, A. Mainwood and K. Osuch, *Phys. Rev. B*, 2007, 76, 155203
- [26] N. Jiang, A. Hatta and T. Ito, *Japanese J. Appl. Phys*, 1998, 37, L1175-L1177
- [27] A. E. Fraser, MSci Undergraduate Thesis, Bristol University, 2012
- [28] M. Z. Othman, PhD Thesis, Bristol University, 2014
- [29] E. B. Lombardi, A. Mainwood, *Diam. Relat. Mater.*, 2008, 17, 1349-1352
- [30] H. Yilmaz, B. R. Weiner, G. Morell, *Diam. Relat. Mater.*, 2007, 16, 840-844
- [31] C. Uzan-Saguy, C. Cytermann, B. Firgeer, V. Richter, R. Brener and R. Kalish, *Phys. Stat. Sol. (A)*, 2002, 193, 508
- [32] R. Zeisel, C. E. Nebel, M. Statzmann, H. Sternschulte, M. Schreck and B. Stritzker, *Phys. Stat. Sol. (A)*, 2000, 181, 45
- [33] O. J. L. Fox, PhD Thesis, Bristol University, 2011
- [34] K. Jagannadham, *Diam. Relat. Mater.*, 2007, 16, 50
- [35] M. Riedel, J. Ristein, and L. Ley, *Phys. Rev. B*, 2004, 69, 125338
- [36] W. Haenni, P. Rycher, M. Fryda and C. Comninellis, *Thin-Film Diamonds Part B*, Academic Press, 2004, 1, 149

- [37] M. Gabrysch, S. Majdi, A. Hallén, M. Linnarsson, A. Schöner, D. Twitchen and J. Isberg, *Phys. Stat. Sol. A*, 2008, 205, 2190
- [38] S. A. Kajihara, A. Antonelli, J. Bernholc and R. Car, *Phys. Rev. Lett.*, 1992, 66, 2010
- [39] M. Nesladek, *Semicond. Sci. Technol.*, 2005, 20, R19-R27
- [40] S. C. Eaton, A. B. Anderson, J. C. Angus, Y. E. Evstefeeva and Y. V. Pleskov, *Electrochem. Solid State Lett.*, 2002, 5, G65
- [41] J. B. Miller, G. R. Brandes, *J. Appl. Phys.*, 1997, 82, 4538
- [42] M. N. R. Ashfold, P. W. May, C. A. Rego, N. M. Everitt, *Chem. Soc. Rev.*, 1994, 23, 21-30
- [43] H. P. Bovenkerk, F. P. Bundy, H. T. Hall, H.M Strong and R. H. Wentorf, *Nature*, 1959, 184, 1094
- [44] Y. Zhang, C. Zang, H. Ma, Z. Liang, L. Zhou, S. Li, X. Jia, *Diamond & Related Materials*, 2008, 17, 209-211
- [45] J. C. Angus, H. A. Will and W. S. Stanko, *J. Appl. Phys.*, 1968, 39, 2915
- [46] F. G. Celii and J. E. Butler, *Annu. Rev. Phys. Chem.*, 1992, 43, 643
- [47] Edited by A. H. Lettington and J. W. Steeds, *Phil. Trans. R. Soc. Lond. A*, 1993, 342, 193
- [48] M. Gabrysch, PhD Thesis, Uppsala University, 2008
- [49] W. S. Lee and J. Yu, *Diamond and Related Materials*, 2005, 14(10), 1647-1653
- [50] P. W. May, C. A. Rego, R. M. Thomas, M. N. R. Ashfold, K. N. Rosser, P. G. Partridge and N. M. Everitt, *J. Mater. Sci. Lett.*, 1994, 13, 247-249
- [51] J. C. Richley, PhD Thesis, Bristol University, 2011
- [52] D. G. Goodwin and J. E. Butler, *Handbook of Industrial Diamond and Diamond Films*, edited by M. A. Prelas, A. Popvici and L. K. Bigelow, Marcel Dekker, Inc., 1998, 527-581
- [53] A. Cheesman, PhD Thesis, Bristol University, 2006
- [54] D. G. Goodwin, J. E. Butler, *Handbook of Industrial Diamonds and Diamond Films*, ed. M. A. Prelas, G. Popovici, L. K. Bigelow, NY: Marcel Dekker, 1997, ch. 11
- [55] P. K. Bachmann, H. J. Hagemann, H. Lade, D. Leers, F. Picht, D. U. Weichert, H. Wilson, *Mater. Res. Soc. Symp. Proc.*, 1994, 339, 267
- [56] A. Edmonds, PhD Thesis, University of Warwick, 2008
- [57] R. H. Telling, C. J. Pickard, M. C. Payne and J. E. Field, *Phys. Rev. Lett.*, 2000, 84, 5160-5163
- [58] D. Huang, M. Frenklach, *J. Phys. Chem.*, 1992, 96, 1868-1875
- [59] S. Koizumi, C. Nebel, and M. Nesládek, *Physics and Applications of CVD Diamond*, Wiley-VCH, Weinheim, 2008
- [60] W. Gordy, W. J. O. Thomas, *J. Chem. Phys.*, 1956, 24, 439
- [61] P.W. May, J. C. Stone, M. N. R. Ashfold, K. R. Hallam, W. N. Wang, N. A. Fox, *Diam. Relat. Mater.*, 1998, 7, 671-676
- [62] B. J. Waclawski, D. T. Pierce, N. Swanson, R. J. Cellota, *J. Vac. Sci. Technol.*, 1982, 21, 368
- [63] B. B. Pate, M. H. Hecht, C. Binns, I. Lindav, W. E. Spicer, *J. Vac. Sci. Technol.*, 1982, 21, 364
- [64] F. J. Himpsel, J. A. Knapp, J. A. von Vechten, D. E. Eastman, *Phys. Rev. B*, 1979, 20(2), 624
- [65] F. Maier, J. Ristein, L. Ley, *Phys. Rev. B*, 2001, 64, 16541
- [66] D. Takeuchi, H. Kato, G. S. Ri, T. Yamada, P. R. Vinod, D. Hwang, C. E. Nebel, H. Okushi, S. Yamasaki, *Appl. Phys. Lett.*, 2005, 86, 152103
- [67] J. B. Cui, J. Ristein, L. Ley, *Phys. Rev. Lett.*, 1998, 81, 429
- [68] O. A. Williams, R. B. Jackmann, *Semicond. Sci. Technol.*, 2003, 18, 34
- [69] L. Diederich, O. M. Kuttel, E. Maillard-Schaller, L. Schlapbach, *Surf. Sci.*, 1996, 349, 176
- [70] Y. Furuya, T. Hashishin, H. Iwanaga, S. Motojim, Y. Hishikawa, *Carbon*, 2004, 42, 331-335
- [71] P. W. May, J. C. Stone, M. N. R. Ashfold, K. R. Hallam, W. N. Wang, N. A. Fox, *Diam. Relat. Mater.*, 1998, 7, 671-676
- [72] B. Rezek, C. E. Nebel, *Diam. Relat. Mater.*, 2006, 15, 1374
- [73] A. Denisenko, A. Aleksov, A. Pribil, P. Gluche, W. Ebert, E. Koln, *Diam. Relat. Mater.*, 2000, 9, 1138
- [74] D. A. Tryk, K. Tsunozaki, T. N. Rao, A. Fujishima, *Diam. Relat. Mater.*, 2001, 10, 1804
- [75] S. J. Sque, R. Jones, *Phys. Rev. B*, 2006, 73, 085313

- [76] K. Larsson, H. Bjorkman, K. Hjort, *J. Appl. Phys.*, 2001, 90, 1026
- [77] A. Laikhtman, A. Hoffman, R. Kalish, Y. Avigal, A. Breskin, R. Chechik, E. Shefer, Y. Lifshitz, *Appl. Phys. Lett.*, 1998, 73, 1433
- [78] P. Atkins, T. Overton, J. Rourke, M. Weller, F. Armstrong, *Shiver & Atkins Inorganic Chemistry*, 4th ed., Oxford University Press, 2006
- [79] R. V. D. Bogerde, BSc. Undergraduate Thesis, University of Bristol, 2012
- [80] H. Haug, S. W. Koch, *Quantum Theory of the Optical and Electronic Properties of Semiconductors*, World Scientific Publishing, 3rd ed., 1994
- [81] G. S. Painter, D. E. Ellis, A. R. Lubinsky, *Phys. Rev. B*, 1971, 4(10), 3610-3622
- [82] L. Diederich, O. M. Kütel, P. Ruffieux, T. Pillo, P. Aebi, L. Schlapbach, *Surf. Sci.* 1998, 417, 41-52
- [83] T. L. Martin, PhD Thesis, Bristol University, 2011
- [84] W. Simone, BSc. Undergraduate Thesis, University of Bristol, 2012
- [85] J. E. Yater, A. Shih, R. Abrams, *J. Vac. Sci. Technol. A*, 1998, 16, 193
- [86] A. D. McNaught, A. Wilkinson, *Compendium of Chemical Terminology*, IUPAC, 1997, 2, 475
- [87] A. Shih, J. Yater, C. Hor, R. Abrams, *Appl. Surf. Sci.*, 1997, 111, 251-258
- [88] C. Bandis, B. B. Pete, *Phys. Rev. Lett.*, 1995, 74(5), 777-780
- [89] S. Katsumata, Y. Oobuchi, T. Asano, *Diam. Relat. Mater.*, 1994, 3, 1296
- [90] N. Kumar, H. Schmidt, C. Xie, *Sol. State. Tech.*, 1995, 38, 71
- [91] I. L. Krainsky, V. M. Asnin, G. T. Mearini, J. A. Dayton, Jr., *Phys. Rev. B*, 1996, 53(12), R7650
- [92] F. Maier, J. Ristein, L. Ley, *Phys. Rev. B*, 2001, 64(16), 165411
- [93] F. Himpsel, J. Knapp, J. van Vechten, D. Eastman, *Phys. Rev. B*, 1979, 20(2), 624-627
- [94] J. van der Weide, Z. Zhang, P. Baumann, M. Wensell, J. Bernhole, R. Nemanich, *Phys. Rev. B*, 1994, 50, 5803
- [95] J. Cui, J. Ristein, L. Ley, *Phys. Rev. Lett.*, 1998, 81(2), 429-432
- [96] R. Kollath, *Secondary Electron Emission of Solids Irradiated by Electrons*, *Encyclopaedia of Physics*, ed. S. Flügge, 1956, 21, 232-303
- [97] L. Diederich, O. Kütel, P. Aebi, L. Schlapbach, *Surf. Sci.*, 1998, 418(1), 219-239
- [98] D. Takeuchi, H. Kato, G. Ri, T. Yamada, P. Vinod, D. Hwang, C. Nebel, H. Okushi, S. Yamaski, *Appl. Phys. Lett.*, 2005, 86(15), 152103
- [99] F. Guthrie, *R. Soc. Proc.*, 1873, 21, 168-169
- [100] R. H. Fowler, L. Nordheim, *Soc. Proc.*, 1928, 117, 549
- [101] J. S. Lapington, D. P. Thompson, P. W. May, N. A. Fox, J. Howorth, J. Milnes, V. Taillandier, *Nucl. Instr. Methods Phys. Res. A*, 2009, 253-257
- [102] J. S. Lapington, V. Taillandier, B. L. Cann, J. Howorth, J. Milnes, R. Vaz, P. W. May, N. A. Fox, R. Stevems, L. Wang, *J. Instrum.*, 2012, 7, E04002
- [103] C. Bandis, B. Pate, *Phys. Rev. B*, 1995, 52, 12056
- [104] G. Wang, S. Bent, J. Russell, M. D'Evelyn, *J. Am. Chem. Soc.*, 2000, 122, 744
- [105] J. Yater, A. Shih, R. Abrams, *Phys. Rev. B*, 1997, 56, 4410
- [106] A. Modinos, *Field, Thermionic and Secondary Electron Emission Spectroscopy*, Plenum Press, 1984, 327
- [107] P. G. Lurie, J. M. Wilson, *Surf. Sci.*, 1977, 65, 476-498
- [108] A. L. Huges, L. A. Dubridge, *Photoelectric Phenomena*, McGraw-Hill, New York and London, 1932
- [109] J. B. Miller, G. R. Brandes, *J. Appl. Phys.*, 1997, 82, 4538
- [110] W. E. Spicer, *Phys. Rev.*, 1958, 112, 114
- [111] O. M. Küttel, P. Aebi, L. Schlapbach, *Surf. Sci.*, 1998, 418, 219-239
- [112] C. N. Berglund, W. E. Spicer, *Phys. Rev.*, 1964, 136, A1030 and A1044
- [113] W. E. Spicer, C. N. Berglund, *Rev. Sci. Instr.*, 1964, 35, 1665
- [114] W. Krolikowski, W. E. Spicer, *Phys. Rev.*, 1969, 185, 882
- [115] C. Bandis, B. B. Pate, *Phys. Rev. Lett.*, 1995, 74(5), 777-780

- [116] V. M. Asnin, I. L. Krainsky, 9th International Vacuum Microelectronics Conference, St. Petesburg, 1996, 354-357
- [117] J. Krása, E. Woryna, M. P. Stöckli, *Meas. Sci. Technol.*, 1998, 9, 1632-1634
- [118] V. E. Henrich, J. C. C. Fan, *Appl. Phys. Lett.*, 1973, 23, 7
- [119] M. P. Seah, *Surf. Sci.*, 1969, 17, 132-160
- [120] J. J. Lander, *Phys. Rev.*, 1953, 91(6), 1382-1387
- [121] R. Emran, BSc Undergraduate Thesis, University of Bristol, 2013
- [122] O. A. Williams, J. Hees, C. Dieker, W. Jäger, L. Kirste, C. E. Nebel, *ACS Nano*, 2010, 4, 4824-4830
- [123] R. J. Hunter, *Zeta Potential in Colloid Science: Principles and Applications*, Academic Press, 1981
- [124] K. Yoshino, J. R. Esmond, D. E. Freeman, W. H. Parkinson, *J. Geo. Research*, 1993, 98, 5205-5211
- [125] J. Hees, A. Kriele, O. A. Williams, *Chem. Phys. Lett.*, 2011, 509, 12-15
- [126] R. Emran, BSc Undergraduate Thesis, University of Bristol, 2013
- [127] N. B. Colthup, L. H. Daly, S. E. Wiberley, *Introduction to Infrared and Raman Spectroscopy*, 2nd edition, 1975
- [128] L. A. K. Staveley, *Characterization of Chemical Purity: Organic Compounds*, IUPAC, 1971
- [129] M. Kelly, PhD Thesis, University of Bristol, 2014
- [130] P. J. Goodhew, J. Humphreys, R. Beanland, *Electron Microscopy and Analysis*, Taylor & Francis, 3rd ed., chapter 5, 2001.
- [131] I. M. Watt, *The Principles and Practice of Electron Microscopy*, Cambridge University Press, 2nd ed., chapter 3, 1985
- [132] L. R. White, *J. Chem. Soc., Faraday Trans 1*, 1977, 73, 390-398
- [133] D. Zhang, R. Q. Zhang, *J. Phys. Chem. B*, 2005, 109, 9006